

REFERENCE COPY

SANDIA REPORT

SAND90-3246 • UC-721

Unlimited Release

Printed June 1991



SAND90-3246
0002
UNCLASSIFIED

06/91
62P

STAC

Evaluation of the Role of Threshold Pressure in Controlling Flow of Waste-Generated Gas into Bedded Salt at the Waste Isolation Pilot Plant

Peter B. Davies

Prepared by
Sandia National Laboratories
Albuquerque, New Mexico 87185 and Livermore, California 94550
for the United States Department of Energy
under Contract DE-AC04-76DP00789

Issued by Sandia National Laboratories, operated for the United States Department of Energy by Sandia Corporation.

NOTICE: This report was prepared as an account of work sponsored by an agency of the United States Government. Neither the United States Government nor any agency thereof, nor any of their employees, nor any of their contractors, subcontractors, or their employees, makes any warranty, express or implied, or assumes any legal liability or responsibility for the accuracy, completeness, or usefulness of any information, apparatus, product, or process disclosed, or represents that its use would not infringe privately owned rights. Reference herein to any specific commercial product, process, or service by trade name, trademark, manufacturer, or otherwise, does not necessarily constitute or imply its endorsement, recommendation, or favoring by the United States Government, any agency thereof or any of their contractors or subcontractors. The views and opinions expressed herein do not necessarily state or reflect those of the United States Government, any agency thereof or any of their contractors.

Printed in the United States of America. This report has been reproduced directly from the best available copy.

Available to DOE and DOE contractors from
Office of Scientific and Technical Information
PO Box 62
Oak Ridge, TN 37831

Prices available from (615) 576-8401, FTS 626-8401

Available to the public from
National Technical Information Service
US Department of Commerce
5285 Port Royal Rd
Springfield, VA 22161

NTIS price codes
Printed copy: A04
Microfiche copy: A01

SAND90-3246
Unlimited Release
Printed June 1991

Distribution
Category UC-721

EVALUATION OF THE ROLE OF THRESHOLD PRESSURE IN CONTROLLING FLOW OF WASTE-GENERATED GAS INTO BEDDED SALT AT THE WASTE ISOLATION PILOT PLANT

Peter B. Davies
Fluid Flow and Transport Division 6344
Sandia National Laboratories
Albuquerque, New Mexico

ABSTRACT

Anoxic corrosion and microbial degradation of contact-handled transuranic waste may produce sufficient quantities of gas over a long time period to generate high pressure in the disposal rooms at the Waste Isolation Pilot Plant (WIPP) repository. Dissipation of pressure by outward gas flow will be inhibited by the low permeability of the surrounding rock and by capillary forces that resist gas penetration into this water-saturated rock. Threshold pressure is the gas pressure required to overcome capillary resistance to initial gas penetration and to the development of interconnected gas pathways that would allow outward gas flow. The primary objectives of this study are to estimate the magnitude of threshold pressure in the bedded salt that surrounds the WIPP repository and to evaluate the role this parameter plays in controlling the outward flow of waste-generated gas. Estimates of threshold pressure have been made based on an empirical correlation of threshold pressure with intrinsic permeability from other low-permeability rock types and on a capillary tube model. These two approaches yield generally consistent estimates, suggesting that threshold pressure in relatively pure halite is 20 to 50 MPa, or larger; threshold pressure in impure halite is 5 to 25 MPa; and threshold pressure in more permeable nonhalite interbeds is 2 to 1/2 MPa, or less. Because of the compounding effect of low threshold pressure and relatively high permeability, the nonhalite interbeds are likely to be the dominant pathways for flow of waste-generated gas away from a pressurized repository. Near the repository, a number of processes occur that may significantly

reduce threshold pressure. Local fracturing and pore dilatation in response to excavation-related stresses creates larger pore apertures. Desaturation occurs as a result of drying, dilatation, and/or exsolution of gas that is dissolved in Salado brine under natural conditions. All of these processes contribute to the development of a zone surrounding the repository that contains pore space that is readily accessible to waste-generated gas due to significantly decreased threshold pressures. The threshold pressure estimates and analyses presented in this report are based primarily on threshold pressure information from low-permeability, nonsalt rock types and must be confirmed with direct, laboratory, and/or in situ measurements specific to the Salado Formation at the WIPP repository. In particular, such measurements should be directed toward the nonhalite interbeds and impure halite.

ACKNOWLEDGMENTS

The author thanks Geoff Freeze, Bob Glass, and Elaine Gorham for their helpful review comments on this report. The author also appreciates review and subsequent discussions of a preliminary version of this report with Rick Beauheim, Susan Howarth, Marsh LaVenue, Dave McTigue, John Pickens, and Steve Webb. Carol Gotway provided helpful guidance in the analysis of uncertainty in the correlation of threshold pressure and intrinsic permeability.

CONTENTS

1.	INTRODUCTION	1
2.	THEORETICAL BACKGROUND ON THRESHOLD PRESSURE	7
3.	TECHNIQUES FOR MEASURING THRESHOLD PRESSURE	13
3.1	Direct Measurements	13
3.2	Indirect Measurements	13
4.	TECHNIQUES FOR ESTIMATING THRESHOLD PRESSURE	17
4.1	Empirical Correlations	17
4.2	Capillary Tube Model	20
5.	THRESHOLD PRESSURE ESTIMATES FOR THE SALADO FORMATION	25
5.1	Estimates Based on Permeability Correlation	25
5.2	Estimates Based on Capillary Tube Model	29
6.	OTHER PROCESSES AND PHYSICAL CHARACTERISTICS THAT MAY INFLUENCE THRESHOLD PRESSURE IN THE WIPP ENVIRONMENT	31
6.1	Threshold Pressure Under Partially Saturated Conditions	31
6.2	Impact of Fracturing on Threshold Pressure	32
6.3	Possibility of Zero Permeability in Undeformed, Pure Halite	33
7.	DISCUSSION	35
7.1	Threshold Pressure Estimates for the Salado Formation	35
7.2	Conceptual Model for Hydrologic Response of the Repository to Waste-Generated Gas	37
8.	REFERENCES	39

FIGURES

1.	Definition of relative permeability to water (brine) and gas as a function of the degree of water (or gas) saturation	3
2.	Schematic illustration of the role of threshold pressure in inhibiting gas flow from a gas-filled disposal room into adjacent low-permeability rock that is brine saturated	4
3.	Definition of threshold pressure and relationship between capillary pressure and relative permeability	11
4.	Plot showing an example of threshold pressure measurement by mercury injection for a 1 microdarcy (10^{-18} m ²) sandstone	14
5.	Plot of threshold pressure versus intrinsic permeability for a wide variety of geologic materials and over a 13 order-of-magnitude range in intrinsic permeability	18
6.	Plot of estimated versus measured threshold pressure for estimates based on the capillary tube model	22
7.	Plot of estimation error versus intrinsic permeability for threshold pressure estimates based on empirical correlation and on the capillary tube model	23
8.	Plot of correlation of threshold pressure with intrinsic permeability for a composite of data from all consolidated rock lithologies	26
9.	Plot summarizing estimated threshold pressure for various lithologic units in the Salado Formation based on correlation with intrinsic permeability	28

TABLES

1.	Highest observed fluid pressures in the Salado Formation	2
2.	Range of threshold pressure parameters for geologic systems	10
3.	Threshold pressure versus intrinsic permeability correlations	19
4.	Parameter values for estimating threshold pressure of the Salado Formation (far-field) based on the capillary tube model	30

1. INTRODUCTION

Analyses of the post-closure evolution of disposal rooms in the Waste Isolation Pilot Plant (WIPP) repository indicate that microbial degradation of organic waste and anoxic corrosion of steel drums and metallic waste may be capable of generating enough gas to pressurize the rooms to lithostatic pressure (Lappin et al., 1989). Recent estimates of gas generation by anoxic corrosion suggest a production rate of 2 moles/drum per year with a total potential of 900 moles/drum (Brush, 1990). Similar estimates for gas generation by microbial activity suggest a production rate of 1 mole/drum per year with a total potential of 600 moles. Gas generation by radiolysis is expected to proceed at a much slower rate. Current gas-generation research is focused on laboratory and in situ experiments that will provide a more accurate prediction of gas-generation rates under brine-inundated conditions and of possible rate reductions under vapor-limited ("humid") conditions. Other in situ measurements and model analyses focus on assessing the hydrologic and mechanical response of the disposal rooms and surrounding Salado Formation to high gas pressure.

An important objective in assessing the hydrologic response to waste-generated gas is determining how much gas can flow from the repository into the surrounding rock mass, thereby regulating gas pressure within the repository. Three physical characteristics of the surrounding rock will control the flow of gas from the repository into the rock. These characteristics are pore fluid pressure, threshold pressure, and gas permeability.

The difference between fluid pressure in pores of the waste and backfill in the repository and fluid pressure in the pores of the surrounding Salado Formation provides the primary driving force for moving gas and brine between these two regions. Current measurements indicate that undisturbed (i.e. far-field) pore pressure in the Salado Formation at the elevation of the repository is between hydrostatic (5.9 MPa) and lithostatic (14.8 MPa) (Peterson et al., 1987; Nowak and McTigue, 1987; Lappin et al., 1989). Highest pore pressures are usually measured in anhydrite interbeds and range from 8.8 to 11.5 Mpa (Table 1). Pore pressures extrapolated from pressure recovery trends yield higher values, ranging from 9.3 to 13.9 MPa (Table 1). Pore pressures are much lower within the first few meters of the excavation surface due to depressurization that accompanies brine flow toward the excavation and/or to dilatation of pores caused by high deviatoric stresses near the excavation.

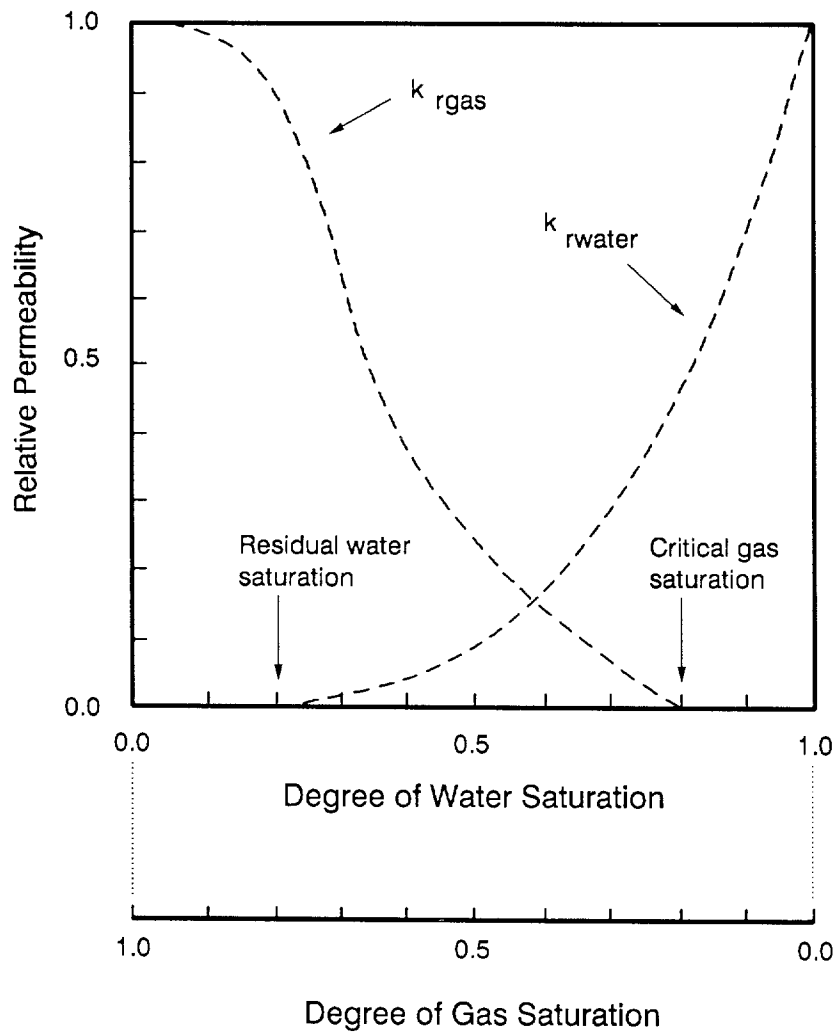
The second characteristic controlling gas flow into the rock is the threshold pressure required to overcome capillary resistance and drive gas into the brine-filled rock pores. Rock that is fully saturated with brine is impermeable to gas (Figure 1) until the capillary forces resisting the penetration of gas into the rock pores have been overcome and a network of interconnected gas pathways has been established. The sum of the existing pore pressure in the rock and the threshold pressure is the gas-pressure level that must be reached in the room before gas can flow from the room into the rock (Figure 2). Because the rock is depressurized within the first few meters of an excavation, the pore-pressure component of this sum will be relatively small. However, for gas penetration beyond the first few meters, the pore-pressure component of this sum is much larger, on the order of 12 MPa or higher as discussed in the previous paragraph.

Table 1. Highest observed fluid pressures in the Salado Formation.

LITHOLOGIC UNIT	DISTANCE FROM EXCAVATION (m)	APPROXIMATE AGE OF EXCAVATION (yr)	HIGHEST MEASURED PRESSURE (MPa)	HIGHEST EXTRAPOLATED PRESSURE (MPa)	REFERENCE
Marker Bed 139	12	2 3/4	10.3	10.3	Peterson et al., 1987
Marker Bed 139	10	5 1/2	8.8	9.3	Beauheim et al., in review
Marker Bed 139	23	1/2	10.5	10.7 - 12.8	Howarth et al., in press
Anhydrite B	22	1/2	11.5	12.8	Howarth et al., in press
Marker Bed 138	24	1/2	9.3	9.3 - 13.9	Howarth et al., in press

The third characteristic controlling the flow of gas from the repository is the permeability of the rock to gas. Gas permeability is a function of the intrinsic permeability of the rock and of the degree of saturation, which controls the relative permeability to gas and brine (Figure 1). When little or no gas is present, the gas phase is not continuous throughout the pore network and, therefore, no interconnected gas flow pathways exist. In this state, the rock is impermeable to gas. Only after sufficient gas is present to create interconnected pathways does the rock become permeable to gas. The fluid saturation corresponding to the incipient development of an interconnected network of gas pathways is commonly referred to as the critical gas saturation or residual equilibrium gas saturation (Figure 1). As gas saturation increases further, relative permeability to gas becomes larger and relative permeability to brine becomes smaller. At high gas saturations, a point is eventually reached where brine is no longer continuous throughout the pore network and relative permeability to brine becomes zero. This point is commonly referred to as the residual water saturation. At high gas saturations, the relative permeability to gas approaches 1.0 and in this state the permeability of the rock to gas approaches the intrinsic permeability.

The physical characteristics of the rock and fluid surrounding the WIPP repository are complex. The Salado Formation contains interbeds of clay and anhydrite, which in situ tests indicate have much higher permeability than the halite (Beauheim et al., in review; Howarth et al., in press).



Definitions:

$$k_{r\text{gas}} = \frac{k_{\text{gas}}}{k}$$

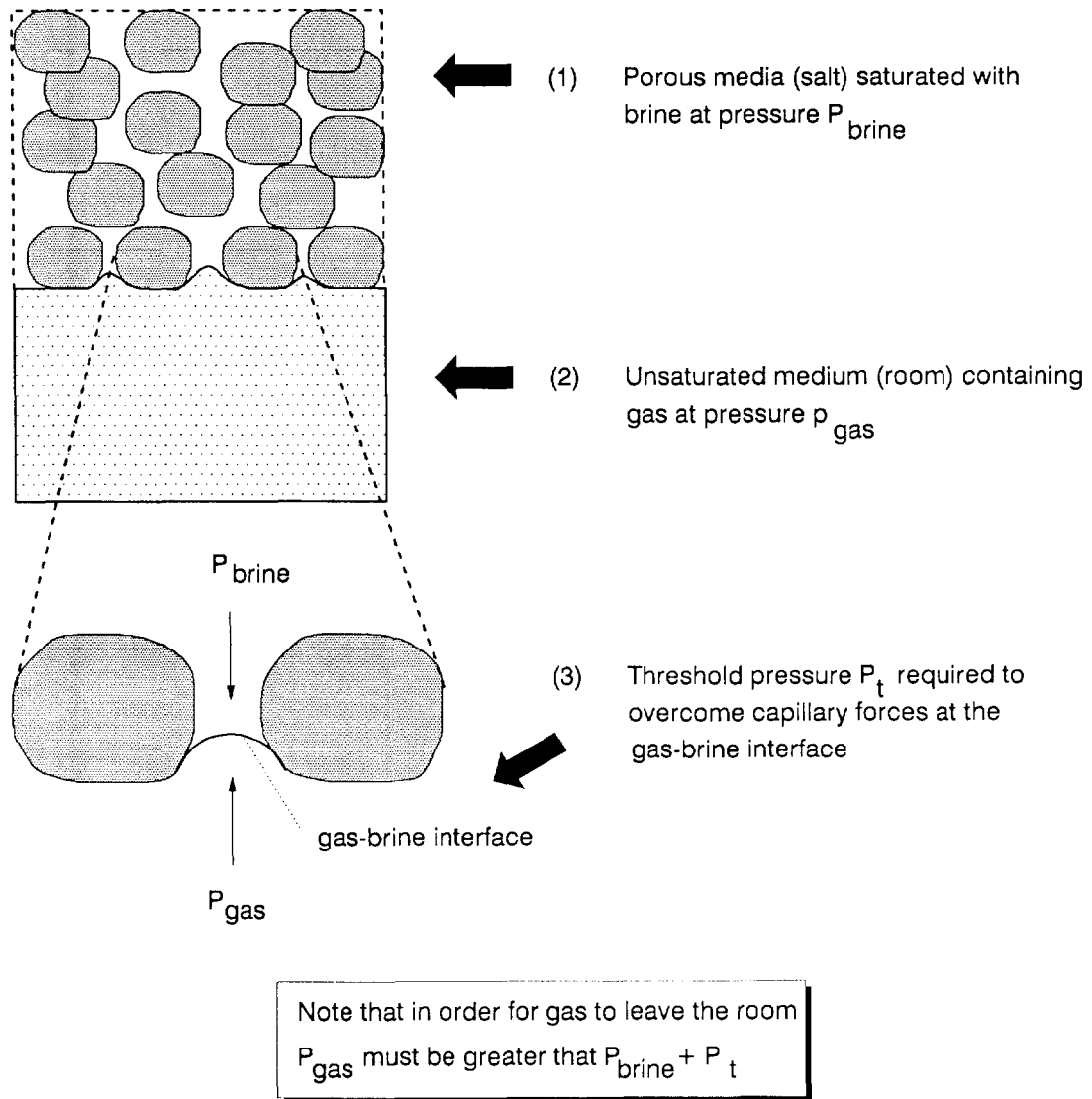
$$k_{r\text{water}} = \frac{k_{\text{water}}}{k}$$

k = intrinsic permeability to a single-phase fluid that completely saturates the medium

Note that at water saturations between the critical gas saturation and 1.0, the rock is impermeable to gas

TRI-6344-723-0

Figure 1. Definition of relative permeability to water (brine) and gas as a function of the degree of water (or gas) saturation. Also note definitions of residual water saturation and critical gas saturation.



TRI-6344-724-0

Figure 2. Schematic illustration of the role of threshold pressure in inhibiting gas flow from a gas-filled disposal room into adjacent low-permeability rock that is brine saturated.

The halite itself contains stratigraphic variations in grain size, texture, and impurity content (mostly clay). In situ tests, laboratory measurements, and brine seepage observations indicate that hydraulic characteristics of the halite units are also variable. In addition to natural variability in the Salado Formation, stress redistribution in response to excavation of the repository has caused near-field changes in hydrologic conditions: dilatation and fracturing have increased intrinsic rock permeability in some locations; brine drainage has decreased pore pressures in the Salado; elastic and inelastic changes in pore volume have caused additional complexity in the near-field fluid pressure distribution; and dilatation, drying, and possible exsolution of dissolved gas that occurs naturally in the Salado brine have caused varying degrees of desaturation (Borns and Stormont, 1988, 1989; Nowak and McTigue, 1997; McTigue et al., 1989; Stormont et al., 1987).

At the June, 1989 National Academy of Sciences WIPP Panel Meeting, John Bredehoeft (U.S. Geological Survey) and George Hornberger (University of Virginia) suggested that because threshold pressure is controlled to a large degree by pore size and because pores in halite are extremely small, threshold pressure may be extremely high. Therefore, the combination of high existing pore pressures and high threshold pressures may create a situation in which the rock surrounding the WIPP repository is effectively impermeable to gas. Concern was expressed that in the absence of gas flow from the repository, pressures may reach or exceed lithostatic and cause fracturing of unpredictable orientation and extent.

As a first step toward assessing potential for gas flow out of the WIPP repository, the objectives of this study are to estimate the magnitude of threshold pressure in the bedded salt that surrounds the WIPP repository and to characterize the role that threshold pressure may play in controlling the outward flow of waste-generated gas. In order to accomplish these objectives, the following discussion is divided into three main segments. The first segment focuses on threshold pressure theory and techniques for measuring and estimating threshold pressure in low permeability environments. The second segment focuses on estimates of threshold pressure for the Salado Formation in the vicinity of the WIPP repository. The third segment focuses on other processes and physical characteristics that may influence threshold pressure in the WIPP environment.

2. THEORETICAL BACKGROUND ON THRESHOLD PRESSURE

When two immiscible fluids such as water and gas are in contact, a discontinuity in pressure exists across the interface that separates them. Water, which tends to adhere to the rock matrix, is referred to as the wetting phase, while the gas constitutes the nonwetting phase. The difference in pressure between these two fluids is called capillary pressure p_c :

$$p_c = p_{\text{gas}} - p_{\text{water}} \quad (1)$$

Capillary pressure is a function of the effective radius r_e of the rock pores, surface tension σ along the interface, and the contact angle α between the interface and the adjacent solid material:

$$p_c = \frac{2 \sigma \cos \alpha}{r_e} \quad (2)$$

Effective radius, r_e , is defined in terms of principle radii r_1 and r_2 , and therefore, is affected by both pore size and pore shape:

$$\frac{2}{r_e} = \left(\frac{1}{r_1} + \frac{1}{r_2} \right) \quad (3)$$

In most analyses involving water with glass or rock, complete wetting of the solid is assumed. Under these conditions, $\cos \alpha$ is equal to one and Equation (2) becomes:

$$p_c = \frac{2 \sigma}{r_e} \quad (4)$$

In order for gas to penetrate a fluid-filled capillary tube or a saturated porous material, pressure in the gas must be high enough to deform the interface to a sufficiently small radius to pass through the tube or rock pores. Pore space in rock is actually a complex arrangement of space with relatively large effective radius, "pores," and space with relatively small effective radius, "necks." Gas penetration into a water-saturated rock is controlled to a large degree by the small effective radius pore space, that is by the necks. In low-permeability rock, the effective radius of necks is very small, and therefore the gas pressure required to overcome capillary forces and permit gas penetration is very large.

One approach to quantifying threshold pressure phenomena in porous media has been to develop an idealized model using a bundle of capillary tubes as the conceptual framework. Based on Poiseuille's Law for laminar flow through an individual capillary tube, Darcy's Law for flow through porous media, and the relationship between capillary pressure and tube radius, the following expression for threshold pressure can be derived (Wyllie and Spangler, 1952; Thomas et al., 1968):

$$P_t = \sigma \left[\frac{T \phi}{k_0 k} \right]^{1/2} \quad (5)$$

where:

P_t = threshold pressure [M/LT²]

σ = surface tension [M/T²]

ϕ = porosity [dimensionless]

k_0 = pore shape factor [dimensionless]

T = tortuosity [dimensionless]

k = intrinsic permeability [L²]

Tortuosity is a measure of the actual length of tortuous flow pathways in a porous medium and is defined in the hydrology literature as follows (Bear, 1972):

$$T = \left[\frac{L}{L_e} \right]^2 \quad (6)$$

where:

L = length of porous system [L]

L_e = length of tortuous flow path through porous system [L]

In order to avoid confusion, it should be noted that the definition of tortuosity in the petroleum literature is the reciprocal of Equation 6 (Rose and Bruce, 1949; Wyllie and Spangler, 1952).

The variation of measured parameter values in Equation 5 is summarized in Table 2 for gas-water systems in geologic settings ranging from unsaturated flow in unconsolidated materials near the ground surface to natural gas reservoirs at depth. By far the dominant parameter controlling threshold pressure over this broad range of geologic environments is intrinsic permeability, which has a range spanning approximately 13 orders of magnitude. Both the capillary model represented by Equation 5 and empirical correlations of threshold pressure versus intrinsic permeability have been widely used in the petroleum industry to make estimates of threshold pressure (Thomas et al., 1968; Katz and Coates, 1968; Katz and Tek, 1970; Ibrahim et al., 1970). These estimation techniques will be discussed in more detail in a later section of this report.

Studies of threshold-pressure phenomena have utilized a variety of techniques to measure nonwetting-phase penetration pressures and a variety of terminology has been applied (Dullien, 1979). In some instances, the definition of threshold pressure contains different assumptions about what constitutes initial "penetration" or "breakthrough" of gas or some other nonwetting phase. Natural materials contain pores of many different sizes and flow along any given pathway may encounter both large radii pores and small radii necks. On a microscopic scale, gas will penetrate into larger pores at lower capillary pressure than is required for penetration through smaller pores or necks with relatively small effective radii. Some investigators define threshold pressure as the capillary pressure associated with first penetration of a nonwetting phase into the largest pores near the surface of the medium. Others define threshold pressure as the capillary pressure associated with the incipient development of a continuum of the nonwetting phase through a pore network, providing gas pathways not only through relatively large pores, but also through necks between pores.

The physical distinction between these two definitions of threshold pressure is illustrated in Figure 3, which shows the relationship between capillary pressure under draining conditions and the corresponding changes in relative permeability to the gas and water phases. Defining threshold pressure as corresponding to first penetration of a nonwetting phase into the largest pores near the surface of the medium means that threshold pressure is equal to the capillary pressure at a water saturation of 1.0. Defining threshold pressure as corresponding to the incipient formation of a continuum of the nonwetting phase through the pore network means that threshold pressure is equal to the capillary pressure at a saturation equal to the critical gas saturation. In other words, threshold pressure is equal to the capillary pressure at which the relative permeability to the gas phase begins to rise from its zero value, corresponding to the incipient development of interconnected gas flow paths through the pore network.

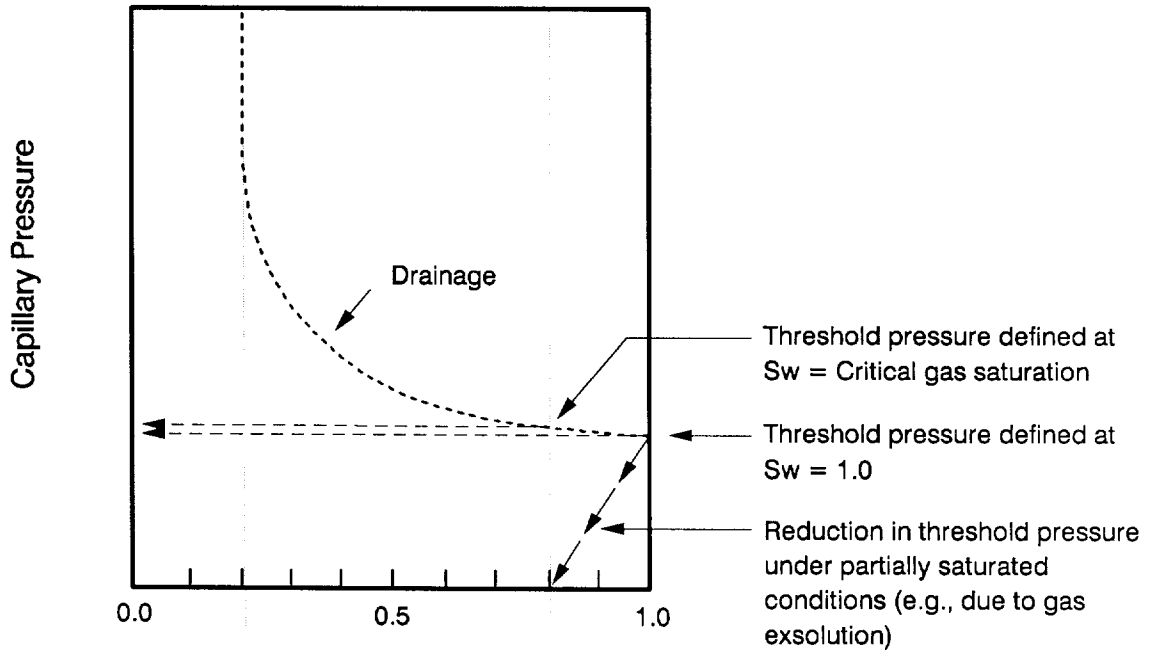
The present study is concerned with the potential for flow of waste-generated gas outward from the WIPP repository. This process will likely require that outward flowing gas penetrate and establish a gas-filled network of flow paths in the surrounding bedded salt. Therefore, the latter definition of threshold pressure being associated with the incipient formation of a continuous network of gas flow paths has been adopted for this study.

Table 2. Range of threshold pressure parameters for geologic systems.

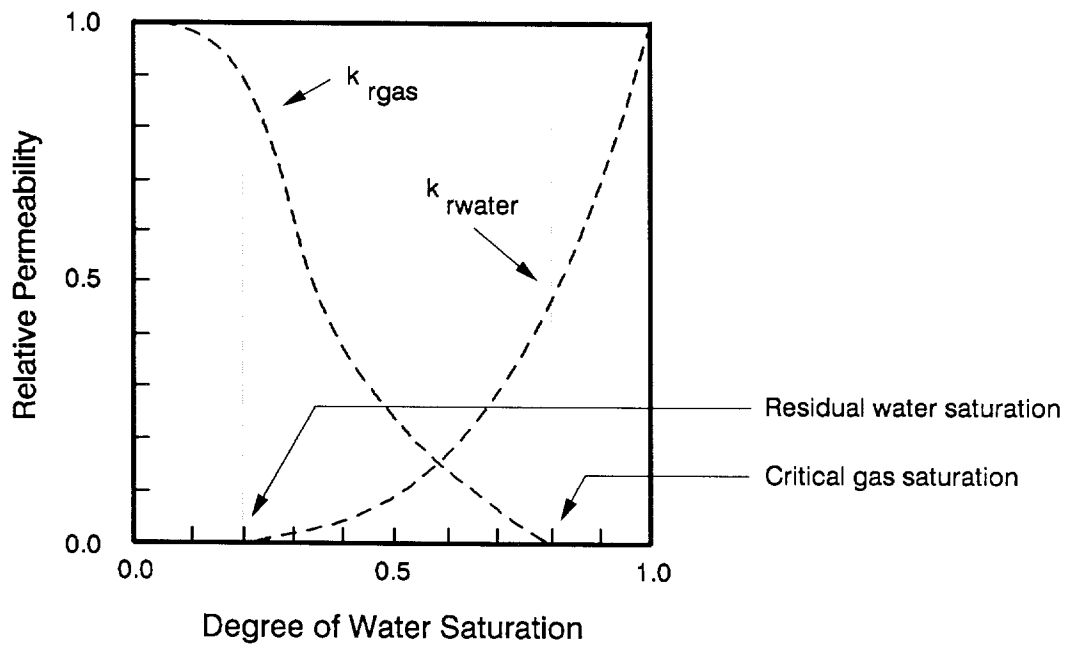
PARAMETER	RANGE	COMMENTS	MAGNITUDE OF RANGE	REFERENCE
Surface tension	Low	0.05 N/m	1.6	Hocott, 1939
	High	0.08 N/m		Weast, 1978
Porosity	Low	0.001	500	Powers et al., 1978
	High	0.500		Freeze and Cherry, 1979
Pore shape factor	Low	2.0	1.5	Wyllie and Spangler, 1952
	High	3.0		Wyllie and Spangler, 1952
Tortuosity	Low	0.02	35	Barker and Foster, 1981
	High	0.70		de Marsily, 1986
Permeability	Low	10^{-22} m^2	10^{13}	Nowak et al., 1988; Ibrahim et al., 1970
	High	10^{-9} m^2		Freeze and Cherry, 1979

As noted previously, threshold pressure phenomena have been studied in a broad range of geologic environments. Studies of unsaturated flow, commonly in high- to intermediate-permeability soils, have used threshold pressure (commonly referred to as "bubbling pressure" or "air-entry pressure" in the unsaturated flow literature) as an indirect measure of the equivalent diameter of the largest neck in a given sample and as a fundamental hydraulic parameter for characterizing unsaturated materials (Brooks and Corey, 1964; Stakman, 1968; Cosby et al., 1984). Studies of oil and gas reservoirs, in a wide range of rock types, have used threshold pressure to characterize the role of capillary pressure in trapping petroleum fluids and in influencing multiphase fluid response to pumping (Hassler et al., 1943; Muskat, 1949; Hubbert, 1953). Studies of underground storage of natural gas (Thomas et al., 1968; Ibrahim et al., 1970) and other fluids such as compressed air (Katz and Lady, 1976) and hydrogen (Carden and Paterson, 1979) have examined threshold pressures in low

Capillary Pressure



Relative Permeability



TRI-6344-725-0

Figure 3. Definition of threshold pressure and relationship between capillary pressure and relative permeability.

to very low-permeability rock in great detail because capillary sealing in the caprock is of critical importance for successful underground storage of gases. These very low-permeability caprock environments are similar in many respects to the very low-permeability environment in the salt surrounding the WIPP repository. Therefore, the following discussions of threshold pressure measurement and estimation draw primarily from research directed toward underground gas storage.

3. TECHNIQUES FOR MEASURING THRESHOLD PRESSURE

Research on threshold pressure in caprocks for underground gas storage reservoirs has produced a variety of techniques for measuring threshold pressures in low-permeability materials. Laboratory measurements of threshold pressure can be divided into two categories: direct measurements and indirect measurements. To date, no techniques for in situ measurement of threshold pressure have been reported.

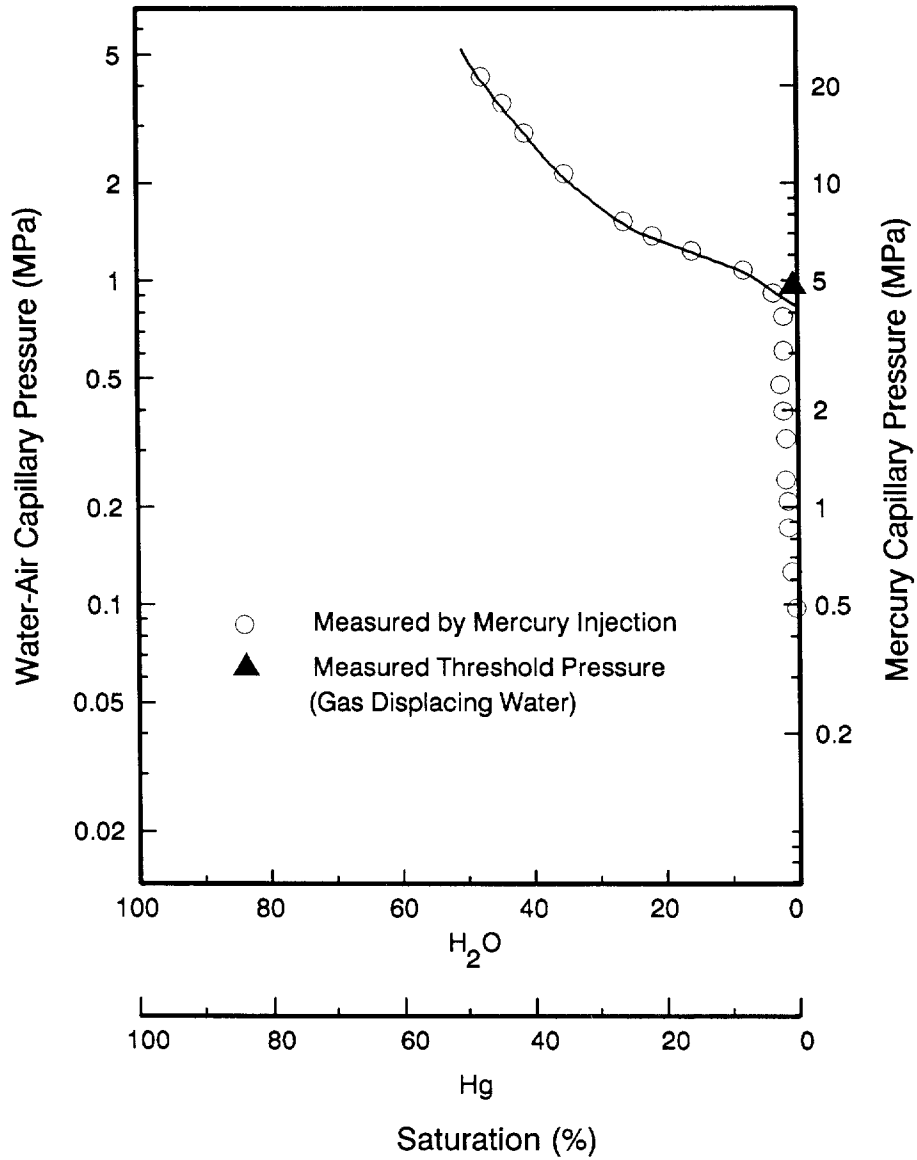
3.1 Direct Measurements

Threshold pressure can be measured directly by incrementally increasing the pressure of gas in contact with the end of a fully saturated core sample and observing the pressure at which gas first penetrates through the core. This approach measures the pressure required for the incipient development of interconnected gas flow paths through the pore network. Direct measurement techniques were first developed by Thomas et al. (1968) and were later enhanced by Ibrahim et al. (1970) and Pandey et al. (1973). In addition to threshold pressure, intrinsic permeability is commonly measured on the same core prior to the threshold pressure measurement. Using these techniques, threshold pressures as high as 14 MPa and intrinsic permeabilities as low as $9 \times 10^{-23} \text{ m}^2$ (approximately 0.1 nanodarcy) have been measured on low-permeability caprock materials (Ibrahim et al., 1970). Caprock lithologies exhibiting high threshold pressures and low permeabilities include anhydrite, carbonate, and shale. No measurements of threshold pressure in bedded salt have been reported in the literature.

3.2 Indirect Measurements

The second category of threshold pressure measurements is based on extrapolating measurements of capillary pressure versus saturation to capillary pressure at a water saturation equal to 1.0. This approach measures the pressure required to initiate gas penetration into the largest pores near the surface of the medium. This technique has been used for a broad range of materials, from high-permeability unconsolidated materials (Brooks and Corey, 1964; Stakman, 1968; Cosby et al., 1984) to low-permeability caprocks (Thomas et al., 1968; Ibrahim et al., 1970). While measurement of the capillary pressure curve in higher permeability materials can be carried out by direct measurements of suction pressure as an initially water-saturated sample is dried, measurement of the capillary pressure curve in low-permeability materials is more difficult.

One technique for measuring capillary pressure curves in low-permeability materials is to measure progressive mercury injection into a dry core sample at successively higher injection pressures (Figure 4). Extrapolation to air-water conditions is accomplished by multiplying by the appropriate capillary pressure ratio for water versus mercury systems (Purcell, 1949; Thomas et al., 1968). A second technique for measuring capillary pressure curves in low-permeability materials is to estimate the pore-size distribution (expressed as effective pore radius) by measuring adsorption of



TRI-6344-726-0

Figure 4. Plot showing an example of threshold pressure measurement by mercury injection for a 1 microdarcy (10^{-18} m^2) sandstone. (Figure adapted from Thomas et al., 1968, Figure 6.)

nitrogen gas in a dry sample (Ibrahim et al., 1970). The corresponding capillary pressure curve is then computed using the relationship between capillary pressure and pore radius expressed in Equation 4. A third technique for measuring capillary pressure curves in low-permeability materials is based on the theoretical relationship between capillary pressure and vapor pressure in the vicinity of a curved vapor-liquid interface (Saito, 1963; Ibrahim et al., 1970). For this technique, vapor pressure in a sealed flask containing a core sample is measured as the degree of saturation is decreased in successive steps. Capillary pressures are then calculated from the theoretical capillary-pressure and vapor-pressure relationship.

Comparison of threshold pressure determinations by direct versus indirect techniques has yielded consistency between techniques to within approximately one-half order of magnitude, or better, for most samples (Thomas et al., 1968; Ibrahim et al., 1970). The dominant approach for determining threshold pressures in low-permeability rock is by direct measurement. An advantage of the direct approach is that intrinsic permeability is readily measured using the same equipment, making acquisition of this important parameter a routine component of the total procedure. An advantage of the indirect technique is that it produces the entire capillary pressure curve, which is also an important piece of information in multiphase flow analysis.

4. TECHNIQUES FOR ESTIMATING THRESHOLD PRESSURE

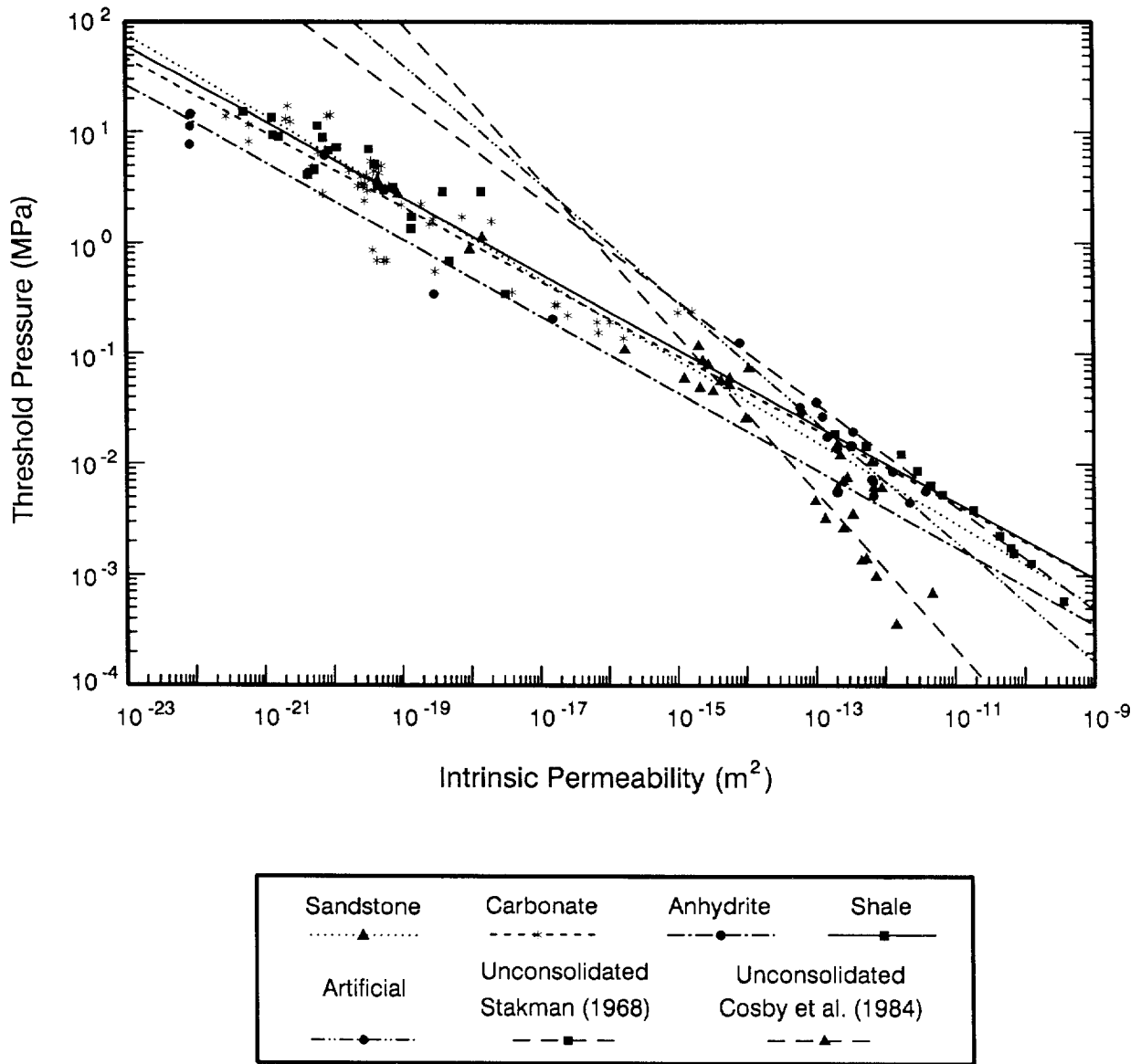
Because laboratory measurement of threshold pressure requires carefully controlled conditions and significant analytic effort, techniques for estimating threshold pressure have been developed as well. Two approaches to threshold pressure estimation have been developed, one based on empirical correlation and the other based on the capillary tube model described in Section 2. In this report and where it appears in the threshold pressure literature, the term "empirical correlation" is used as a general description for an empirical model (describing the relationship between threshold pressure and intrinsic permeability) rather than as a specific statistical quantity associated with correlation coefficients.

4.1 Empirical Correlations

Correlations of threshold pressure with intrinsic permeability have been presented in the soils literature for unconsolidated materials (Stakman, 1968) and in the petroleum literature for consolidated rock (Thomas et al., 1968; Ibrahim et al., 1970). The physical rationale behind this approach is that both threshold pressure and intrinsic permeability are strongly related to pore size and pore interconnections in some fashion. As noted in the previous discussion of the capillary tube model, over the broad spectrum of geologic environments, intrinsic permeability ranges over 13 orders of magnitude (Table 2) and is the dominant factor controlling threshold pressure. The parameter with the second largest range (2-1/2 orders of magnitude) is porosity. Empirical correlations for threshold pressure that incorporate both intrinsic permeability and porosity have also been tested, but show no significant improvement in fit over correlations that use only intrinsic permeability (Ibrahim, 1970).

A detailed literature review has yielded threshold pressure and intrinsic permeability data for a broad range of lithologies with permeabilities ranging from approximately 1×10^{-9} to $1 \times 10^{-22} \text{ m}^2$ (1000 darcies to 0.1 nanodarcy). Most data at the lower end of this range come from measurements on caprock lithologies associated with underground gas storage research. Data at the high end of this range are primarily from unconsolidated soils and artificial porous media. Figure 5 is a plot of threshold pressure versus intrinsic permeability, grouped by lithology. This plot contains only data from research laboratory measurements carried out under carefully controlled conditions. Data from commercial laboratories were not included because of the frequent absence of lithologic information and uncertainty in the range of quality control in the measurements. Data from Cosby et al. (1984) for unconsolidated materials have been presented as a separate curve because these data represent mean values from a large number of samples in groups of different textural classifications rather than individual sample points.

The empirical correlations presented in Figure 5 and summarized in Table 3 reveal a distinct similarity in threshold-pressure versus intrinsic-permeability relationships for the consolidated



TRI-6344-727-0

Figure 5. Plot of threshold pressure versus intrinsic permeability for a wide variety of geologic materials and over a 13 order-of-magnitude range in intrinsic permeability. Data references are summarized in Table 3.

Table 3. Threshold pressure versus intrinsic permeability correlations.

LITHOLOGIC GROUP	NUMBER OF SAMPLES	EXPONENT ⁽¹⁾ (b)	COEFFICIENT ⁽¹⁾ (a)	GOODNESS-OF-FIT (R ²)	DATA REFERENCES
CONSOLIDATED LITHOLOGIES					
Carbonate	49	-0.336	8.7×10^{-7}	0.80	Thomas et al., 1968; Ibrahim et al., 1970
Anhydrite	7	-0.348	2.6×10^{-7}	0.90	Ibrahim et al., 1970
Shale	22	-0.344	7.6×10^{-7}	0.74	Ibrahim et al., 1970
Sandstone	22	-0.369	2.5×10^{-7}	0.97	Thomas et al., 1968; Wyllie & Rose, 1950; Rose and Bruce, 1949
OTHER LITHOLOGIES					
Unconsolidated (2)	11	-0.706	3.7×10^{-12}	0.65	Cosby et al., 1984
Unconsolidated (3)	12	-0.464	3.3×10^{-8}	0.97	Stakman, 1968
Artificial	18	-0.540	2.3×10^{-9}	0.81	Wyllie & Rose, 1950; Rose and Bruce, 1949
COMPOSITE OF CONSOLIDATED LITHOLOGIES					
	100	-0.346	5.6×10^{-7}	0.93	
FOOTNOTES:					
(1) Exponent (b) and coefficient (a) refer to Equation 7.					
(2) Data are mean values for a large number of samples in groups of different soil textural classification.					
(3) Data are actual values for sand samples sorted by grain size.					

lithologies, which include sandstone, shale, carbonate, and anhydrite. These data have been fit with a power curve of the form:

$$y = a x^b \quad (7)$$

The best fit power curves for these lithologies are quite similar, with exponents ranging from -0.34 to -0.37 and coefficients ranging from 3×10^{-7} to 9×10^{-7} . On the other hand, the curves for the high permeability lithologies (unconsolidated soils and artificial porous media) are different, with exponents ranging from -0.46 to -0.71 and coefficients ranging from 3×10^{-8} to 3×10^{-12} . The exponents for the best fit power curves for all lithologies are generally similar to the theoretical -0.50 exponent indicated by the capillary tube model (Equation 5). The Stakman (1968) data for sorted sand are characterized by a close fit (R^2 is equal to 0.97) and by an exponent (-0.46) that is quite similar to the theoretical -0.50 value. Exponents for the consolidated lithologies are all close to -0.35, suggesting that factors other than intrinsic permeability may exert secondary influence on the correlation for consolidated materials.

4.2 Capillary Tube Model

A second approach to estimating threshold pressure is based on the capillary tube model (Equation 5) that explicitly incorporates the influence of additional parameters beyond intrinsic permeability. An objective of Thomas et al. (1968) in developing the capillary tube model for threshold pressure was to develop a model in which all of the parameters are readily measured. Of the parameters in the capillary tube model expressed in Equation 5, only pore shape factor and tortuosity cannot be measured directly. Because the pore shape parameter appears as a square root in Equation 5 and its expected range is very small compared to other parameters (Table 2), this parameter has little impact on calculated threshold pressures.

While tortuosity cannot be measured directly, it can be determined indirectly using electrical resistivity measurements. The tortuous path length, L_e , of fluid flow can be indirectly measured by measuring the flow of electrical current along the same path (Wyllie and Spangler, 1952; Calhoun, 1953; Katz et al., 1957). In a porous medium saturated with a conducting fluid such as brine, the flow of electrical current is almost entirely through the fluid with negligible flow through the solid matrix. Since electrical current is conducted only through the fluid within the porous medium, the resistivity of a saturated sample is higher than the resistivity of the fluid alone. The ratio between the resistivity of a fully saturated porous medium to the resistivity of the saturating fluid is called the "formation factor," F . Because the flow of electricity is analogous to the flow of a fluid with zero viscosity, pore diameters do not affect electrical current flow. Therefore, formation factor depends only on flow path length and porosity (Wyllie and Spangler, 1952):

$$F = \frac{\rho_s}{\rho_l} = \frac{1}{\phi} \left[\frac{L_e}{L} \right] \quad (8)$$

where:

ρ_s = resistivity of saturated porous media

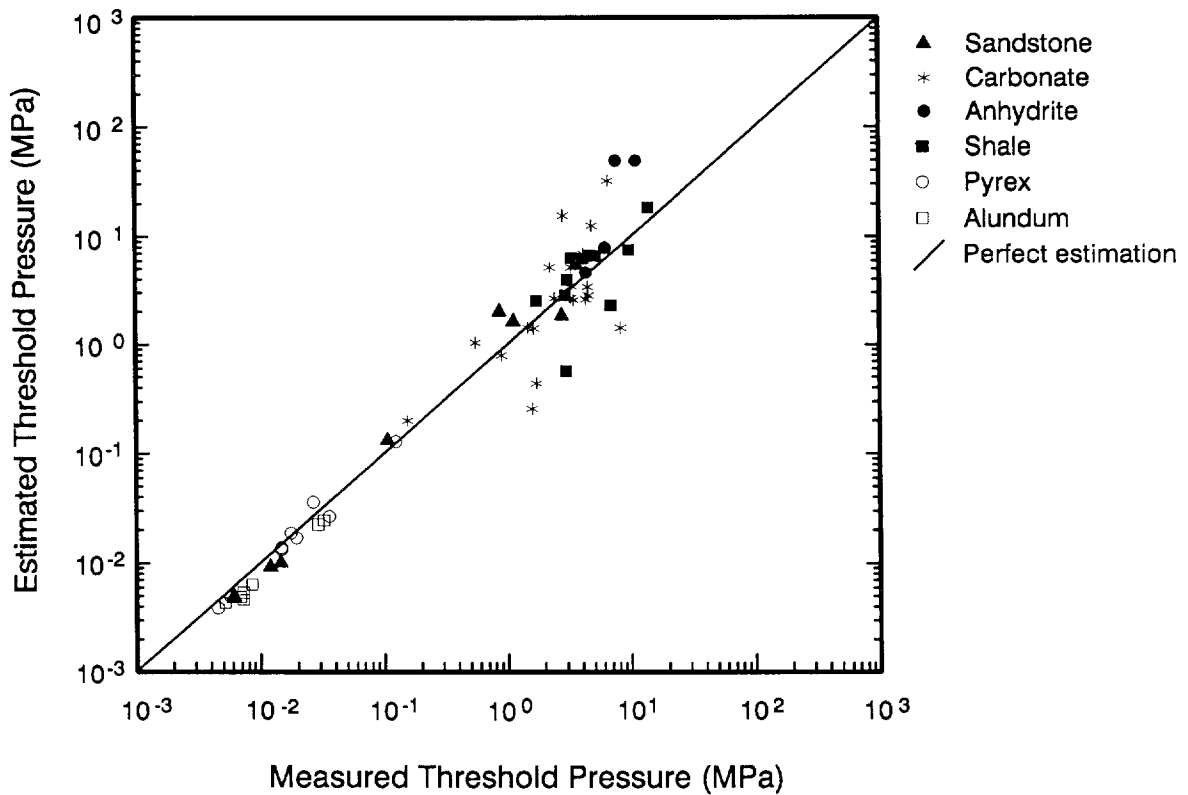
ρ_l = resistivity of the saturating liquid

Bear (1972) has derived a relation between formation factor and tortuosity that differs somewhat from the relation implied by Equations 6 and 8. The Wyllie and Spangler (1952) relation is used here for consistency with the original derivation of the capillary tube model by Thomas et al. (1968).

Using formation factor as a measure of tortuosity, Equations 6 and 8 are substituted into the capillary pressure model expressed in Equation 5 to yield an expression for threshold pressure in which all significant parameters are readily measurable (Thomas et al., 1968):

$$P_t = \frac{\sigma}{F} \left[\frac{1}{k_0 \phi k} \right]^{1/2} \quad (9)$$

Use of Equation 9 requires a more extensive suite of data than is required for the threshold-pressure versus intrinsic-permeability correlations and, therefore, fewer data are available for testing this model than are available for the empirical correlations. Figure 6 is a plot of estimated versus measured threshold pressures for the capillary tube model. Data for this plot are from four consolidated rock types (sandstone, shale, anhydrite, and carbonate) and two artificial porous materials (pyrex and alundum). The data span intrinsic permeabilities from approximately 10^{-12} to 10^{-22} m^2 (1 darcy to 0.1 nanodarcy) and measured threshold pressures ranging from approximately 5×10^{-3} to 1.4×10^1 MPa. For materials with threshold pressures less than about 1 MPa, estimations based on the capillary tube model are quite accurate. Estimations are less accurate for materials with threshold pressures greater than 1 MPa. Six samples have estimated threshold pressures that are above 10 MPa. For all of these samples, measured threshold pressure is less than the estimated value. This discrepancy could reflect difficulties in measuring threshold pressures that exceed 10 MPa or larger uncertainties in the associated measurements of very low permeability (less than 10^{-20} m^2). Alternatively, this discrepancy, and perhaps the wider scatter above 1 MPa, could reflect changes in the pore structure or interactions between pore fluid and pore walls in very tight materials that are not accounted for in the capillary tube model.



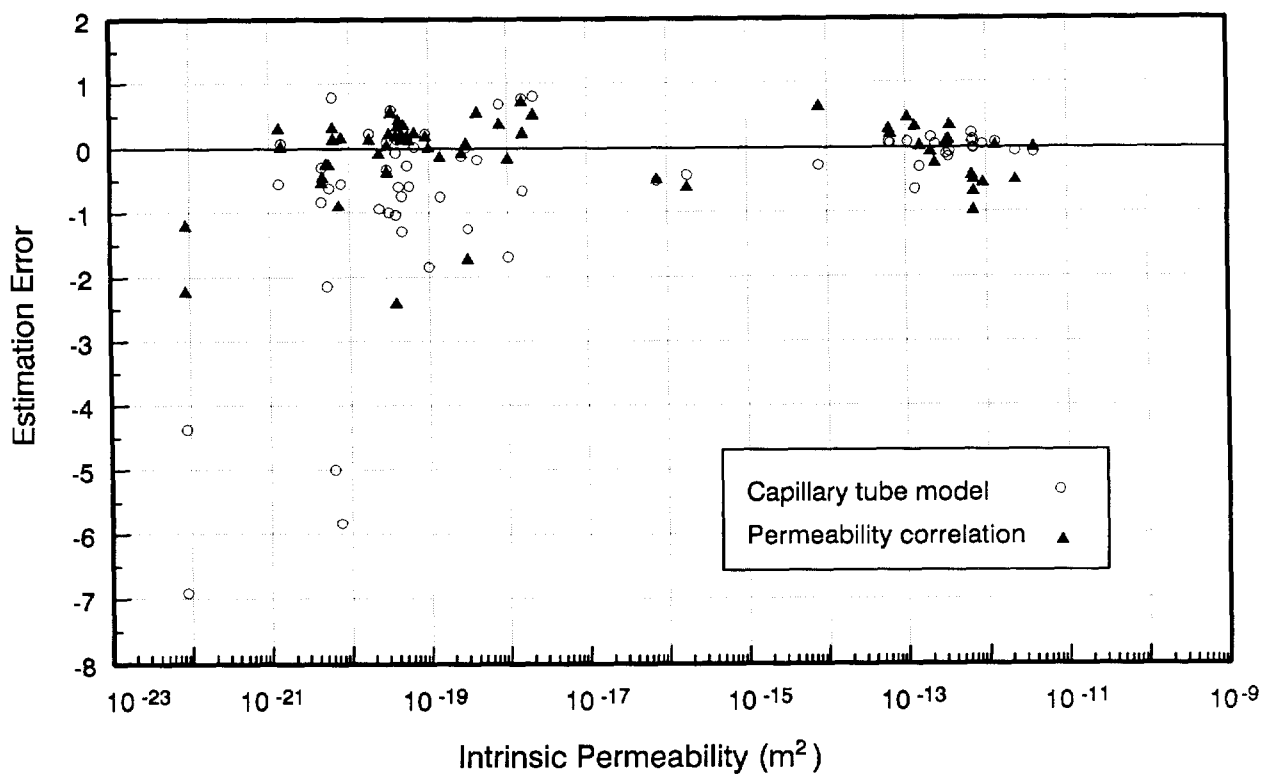
TRI-6344-728-0

Figure 6. Plot of estimated versus measured threshold pressure for estimates based on the capillary tube model. Data are from Thomas et al. (1968), Wyllie and Rose (1950), and Ibrahim et al. (1970).

Because threshold pressure estimations based on the capillary tube model appear to be less accurate at the low permeability end of the range, a comparison of the relative accuracy of estimations based on intrinsic permeability correlations versus estimations based on the capillary tube model has been carried out. For this comparison, estimation error has been defined as follows:

$$P_{t-error} = \frac{P_{t-measured} - P_{t-estimated}}{P_{t-measured}} \quad (10)$$

Figure 7 is a plot of estimation error as a function of intrinsic permeability. This plot illustrates that for samples with permeability greater than 10^{-17}m^2 , both methods produce estimation errors less than 1. In this permeability range, the capillary tube model produces somewhat more accurate estimations. For samples with permeability less than 10^{-17}m^2 , both methods produce larger estimation errors, with a tendency to significantly overestimate threshold pressure in some samples. At this low permeability end of the range, estimations based on the intrinsic permeability correlation appear to be more accurate.



$$\text{Estimation error} = (P_{t \text{ measured}} - P_{t \text{ estimated}}) / P_{t \text{ measured}}$$

TRI-6344-729-0

Figure 7. Plot of estimation error versus intrinsic permeability for threshold pressure estimates based on empirical correlation and on the capillary tube model.

5. THRESHOLD PRESSURE ESTIMATES FOR THE SALADO FORMATION

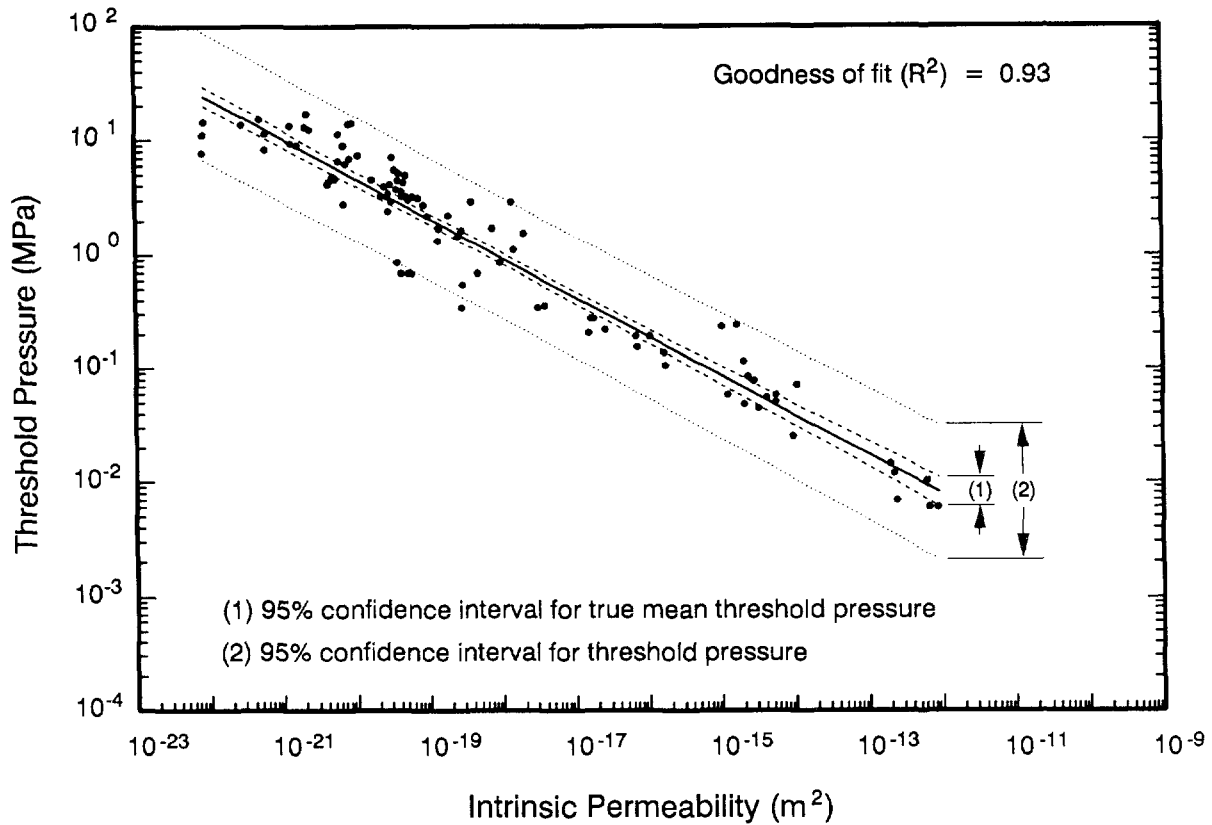
As noted previously, threshold pressure may be an important parameter controlling the flow of waste-generated gas into the rock surrounding the waste-disposal rooms at the WIPP repository. Based on a model of rock pores as uniform tubes and estimates of pore apertures, Stormont et al. (1987) estimated that the threshold pressure for intact halite is somewhere in the range from 100 to less than 1 MPa. In order to further evaluate this parameter for the WIPP environment, estimates of its magnitude have been made using the techniques described in previous sections of this report and existing knowledge of the physical characteristics of the Salado Formation.

5.1 Estimates Based on Permeability Correlation

The Salado Formation, which consists of thick halite beds with anhydrite and clay interbeds, is similar in many respects to the consolidated lithologies presented in Figure 5. Halite, anhydrite, and low-permeability carbonates are all characterized by relatively tight crystalline textures with interconnected pore space occurring along grain boundaries and possibly associated with small fractures. Low-permeability sandstones may also have similarities in pore structure, with crystalline cements filling much of the original open intergrain pore space. The pore structure of clay interbeds of the Salado is expected to be generally similar to that of shales, with platy clay minerals aligned parallel to bedding planes. Given these general similarities, a best-fit power curve through the combined data set for consolidated lithologies was judged to provide the best available correlation for providing estimates of threshold pressure for the Salado Formation (Figure 8; Table 3). This correlation yields the following relationship between threshold pressure and intrinsic permeability:

$$P_t (MPa) = 5.6 \times 10^{-7} [k (m^2)]^{-0.346} \quad (11)$$

Permeability measurements in the Salado Formation have been the focus of significant effort over the course of the WIPP project. In order to address the inherent difficulties in measuring permeability in such tight rock, measurement techniques have evolved over time with significant improvements in both accuracy and lower limits of resolution. Most of the early measurements made in deep boreholes from the ground surface have subsequently been determined to be unreliable because of poorly defined pretest conditions and/or problems with analytic techniques (Lappin et al., 1989; Beauheim et al., in review). In the one surface-based test considered reliable, only an upper bound on the composite permeability of the Marker Bed 138 to Marker Bed 139 interval ($< 3 \times 10^{-19} m^2$) was determined (Beauheim, 1986). Given the difficulties with surface-based measurements, efforts in recent years have focused exclusively on tests in holes drilled directly into the Salado Formation from the WIPP shafts and underground workings.



TRI-6344-730-0

Figure 8. Plot of correlation of threshold pressure with intrinsic permeability for a composite of data from all consolidated rock lithologies. Data are from Ibrahim et al., 1970; Rose and Bruce, 1949; Thomas et al., 1968; and Wyllie and Rose, 1950.

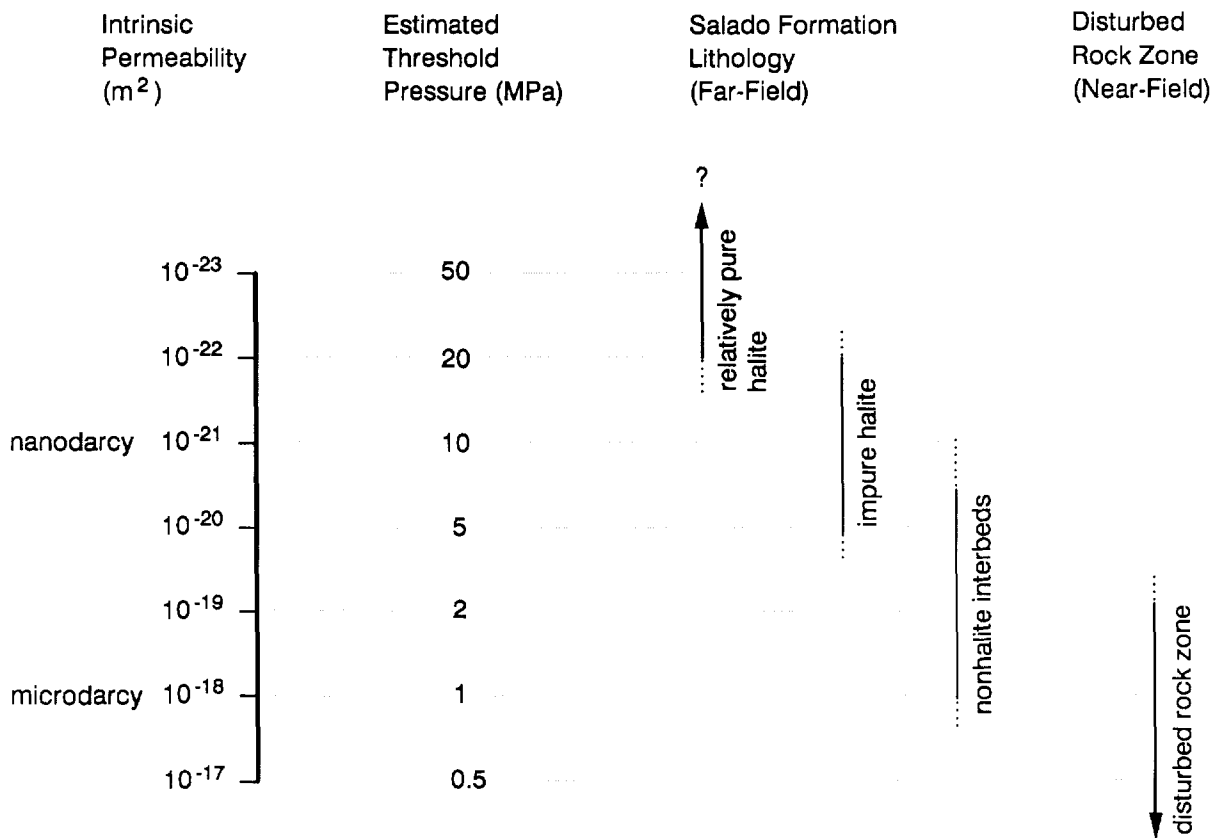
Early underground permeability measurements used gas (nitrogen) injection techniques (Peterson et al., 1985). Complexities in quantifying some of the critical assumptions underlying the interpretation of "gas permeabilities," such as the unknown degree of saturation (Stormont et al., 1987), led to a gradual shift in testing approach to the use of brine-based methods (Peterson et al., 1987; Saulnier and Avis, 1988; Beauheim et al., in review; and Howarth et al., in press). Currently, in situ test activities are focused on permeability measurements in specific stratigraphic units and on the permeability and pore-pressure distribution in the vicinity of a large-scale brine inflow experiment. In addition to measurements designed specifically to determine permeability,

measurements of brine inflow into open observation holes and into controlled experimental holes have also been used to estimate permeability of the surrounding rock (Nowak et al., 1988).

Because both the stratigraphically oriented permeability testing and large-scale brine experiment are ongoing programs, understanding of the permeability distribution in the vicinity of the WIPP disposal rooms is expected to continue to evolve over the next few years. Given the results to date from these ongoing programs and previous permeability measurements, the present understanding of the permeability distribution can be summarized as follows (Figure 9). Permeability within the first two to three meters of an excavation has been increased significantly by near-field deformation effects. Within this zone, permeability is commonly larger than 10^{-19} m^2 (>0.1 microdarcy) and local fracture zones have significantly larger permeabilities. Relative to far-field gas flow, however, permeability and threshold pressure beyond the disturbed rock zone are of primary interest. Far-field permeability in some of the relatively pure halite units is less than 10^{-23} m^2 (<0.01 nanodarcy). Permeability in halite units that contain impurities and/or that may have experienced minor amounts of excavation-related deformation is generally in the range from 10^{-20} to 10^{-22} m^2 (10 to 0.1 nanodarcy). Permeability of Marker Bed 139 and other nonhalite interbeds is highly variable. In some locations, interbed permeability is not significantly different from that of impure halite. In other locations, measured permeabilities of interbeds, most notably in Marker Bed 139, are much higher than that of the halite units. Preliminary results indicate that some interbed permeabilities are as high as 10^{-18} m^2 (1 microdarcy) (Beauheim et al., in review).

Estimated threshold pressures based on the empirical correlation presented in Equation 11 and Figure 8 are summarized in Figure 9. This empirical correlation suggests that threshold pressures in tight, relatively pure halites are larger than 20 MPa. Threshold pressure in pure halite with permeability less than 10^{-23} m^2 may be larger than 50 MPa. Threshold pressures in impure halite, halite that may have experienced small amounts of deformation, and relatively tight interbed units are in the range from approximately 5 to 25 MPa. Threshold pressures in more permeable interbed units are in the range from 1 to 2 MPa. Threshold pressure within the disturbed rock zone is likely to be 2 MPa or significantly less.

Threshold pressure estimates based on the empirical correlation presented in Equation 11 have uncertainty associated with the correlation itself and with factors external to the correlation. One uncertainty in the correlation is the error associated with estimating the true mean value of the threshold pressure for a given intrinsic permeability. Because of the relatively strong correlation (goodness-of-fit, R^2 , is equal to 0.93), the estimation error is fairly small (Figure 8). A second uncertainty in the correlation is prediction error due to random variations in threshold pressure in any given rock type and to measurement error in the original data. Because measurement error in the original data was not quantified, these two sources of uncertainty cannot be evaluated independently. The interval between the bounds of this prediction error is approximately three times the estimated mean threshold pressure (Figure 8). One source of uncertainty external to the correlation is the uncertainty associated with measurements of intrinsic permeability in various lithologies of the



TRI-6344-731-0

Figure 9. Plot summarizing estimated threshold pressure for various lithologic units in the Salado Formation based on correlation with intrinsic permeability.

Salado Formation. Beauheim et al. (in review) estimate the uncertainty in their recent Salado permeability measurements to be approximately one half order of magnitude. Uncertainty in the other Salado permeability measurements (Nowak et al., 1988; Howarth et al., in press) has not yet been quantified. Another very important source of uncertainty is the fact that while the data for the correlation span a wide range of consolidated rock types (shale, anhydrite, carbonate, and sandstone), the data do not include any actual measurements from the Salado Formation at the WIPP repository nor do the data include any actual measurements on halite. At this time, it is not possible to quantify the total uncertainty associated with these estimates. Clearly the total uncertainty is quite large and could be reduced significantly by making direct threshold pressure measurements for selected lithologic units of the Salado Formation.

5.2 Estimates Based on Capillary Tube Model

A second approach for estimating threshold pressure in the Salado Formation is to use the capillary tube model expressed in Equation 9. The advantage of this approach is that the capillary tube model provides a more rigorous accounting for the range of physical properties that may influence threshold pressure. One disadvantage of applying this model is that the Salado is a heterogenous formation and values for the complete parameter suite are not currently available for each of the halite and interbed lithologies. Therefore, threshold pressures estimated using the capillary tube model are limited to rough estimates of the gross characteristics of the formation. A second disadvantage of applying this model is that all Salado permeabilities are less than 10^{-17}m^2 , which is the range where the capillary tube model produces somewhat less accurate estimations (Section 4.2 and Figure 7).

Except for formation factor, all of the capillary tube parameters are available for the Salado Formation. An estimate for formation factor can be derived from in situ geophysical measurements. A best estimate of resistivity of the Salado beyond the disturbed rock zone is 120 ohm-meters, which represents the midpoint of the range estimated for 10 to 20 meters out from the excavation using EM-34 electro-magnetic surveys and is within the dominant 100 to 300 ohm-meter range of apparent resistivity measured using DC electric surveys (Skokan et al., 1989). Resistivity of saturated NaCl brine is 0.044 ohm-meter (Asquith, 1982). Using these values, Equation 8 yields a best estimate of average formation factor of 2.7×10^3 for the Salado Formation.

Table 4 summarizes best estimates and associated rationales for parameter values describing the gross physical characteristics of the Salado Formation. These best estimates are considered representative of impure halite, which comprises more than 50 percent of the Salado in the immediate vicinity of the repository. Using these values, the estimated threshold pressure based on the capillary tube model is 5 MPa. Given the large range of permeabilities in different lithologies and uncertainty in porosity and formation resistivity factor, this threshold pressure could easily be at least an order of magnitude higher (50 MPa) in stratigraphic units consisting of relatively pure halite and at least an order of magnitude lower (0.5 MPa) in some of the nonhalite interbeds. This 0.5 to 50 MPa range is similar to the range estimated using the intrinsic-permeability correlation.

Table 4. Parameter values for estimating threshold pressure of the Salado Formation (far-field) based on the capillary tube model.

PARAMETER	ESTIMATED VALUE	UNITS	RATIONALE	REFERENCE
SURFACE TENSION				
Best estimate	0.07	N/m	Water in contact with air at 20 deg. C	1
Maximum	0.08	N/m	Increase due to dissolved NaCl in saturated brine	1
Minimum	0.05	N/m	Increased pressure (15 MPa), natural gas in water	2
PORE SHAPE FACTOR				
Best estimate	3	-	Shape factor value for high aspect ratio pore space	3
Maximum	3	-	Shape factor value for high aspect ratio pore space	3
Minimum	2	-	Shape factor value for circular pores	3
FORMATION FACTOR				
Best estimate	2.7×10^3	-	Midpoint of EM-34 range, in max. cluster DC meas.	4
Maximum	2.5×10^4	-	High end of DC measurement resistivity range	4
Minimum	2.5×10^2	-	Low end of DC measurement resistivity range	4
POROSITY				
Best estimate	0.01	-	Best estimate, weight loss from heating	5
Maximum	0.05	-	High end of range from EM and resistivity meas.	4
Minimum	0.001	-	Low end of range from drying data	6
PERMEABILITY				
Best estimate	10^{-21}	m^2	Midpoint of range for impure halite	7, 8
Maximum	10^{-18}	m^2	Approx. high end of range for thin interbed zones	7
Minimum	$<10^{-23}$	m^2	Approx. low end of range for relatively pure halite	7, 8

- References: 1 Weast, 1978
2 Hocott, 1939
3 Wyllie and Spangler, 1952
4 Skokan et al., 1989
5 Black et al., 1983
6 Powers et al., 1978
7 Beauheim et al., in review
8 Howarth et al., in press

6. OTHER PROCESSES AND PHYSICAL CHARACTERISTICS THAT MAY INFLUENCE THRESHOLD PRESSURE IN THE WIPP ENVIRONMENT

The preceding discussions focus on threshold pressure in fully saturated, porous media. Other processes and physical characteristics that occur in the WIPP environment may have an impact on threshold pressure. Potentially important processes include partial desaturation and fracturing of rock adjacent to the excavations. A potentially important physical characteristic is the possibility that undeformed, relatively pure halite (i.e., relatively pure halite units located beyond the near-field zone experiencing excavation-related deformation) actually has zero permeability.

6.1 Threshold Pressure Under Partially Saturated Conditions

A combination of geophysical measurements and gas-injection tests suggests that some portion of the rock in the immediate vicinity (i.e. first few meters) of the WIPP excavations may be partially saturated (Stormont et al., 1987; Borns and Stormont, 1988). Processes that may contribute to desaturating rock near the excavations include dilatation, drying, and exsolution of dissolved gas present in Salado brine.

Dilatation is an increase in the size of existing pores or the creation of new pore space by opening along grain boundaries and/or microfracturing that occurs in response to the strongly modified stress field adjacent to an excavation (Jaeger and Cook, 1976; Golder Associates, Inc., 1987). The drop in fluid pressure associated with increased pore volume may draw air into the pores (near the surface of the excavation) and/or may cause dissolved gas in the pore fluid to come out of solution. In either case, an important by-product of dilatation may be the creation of partially saturated pores.

Drying in a porous medium initially occurs as vaporization at the surface of the medium in contact with unsaturated air (McCabe et al., 1985). As water at the surface is depleted, water from the interior is drawn to the surface by capillary forces in the smaller pores, while larger pores in the interior are drained and air enters to replace the displaced water. Once the larger pores are drained, capillary forces in the smaller pores become large enough to move the primary drying surface into the interior of the medium. In a fractured porous medium, early drainage of relatively large aperture fractures may effectively extend active drying surfaces into the interior of the medium, thereby enhancing the overall drying process.

The exsolution of dissolved gas (primarily nitrogen) that occurs naturally in the Salado brine is a third process that may contribute to the creation of partially saturated conditions. In the WIPP mine, the presence of gas is manifested in several ways: 1) gas is observed exsolving in brine weeps on some walls of the excavation; 2) gas is present in many brine samples; 3) gas bubbles are observed in some of the brine observation holes; 4) gas has been encountered in some pressurized test intervals within the Salado; and 5) gas is present in fluid inclusions within individual halite crystals (Peterson et al., 1985; Stein and Krumhansl, 1986; Deal and Case, 1987; Beauheim et al., in review). These

observations indicate that brine from the Salado Formation contains dissolved gas that comes out of solution as fluid pressure is decreased. If gas exsolution is occurring within the Salado, an important by-product of this process is its contribution to decreasing the degree of water saturation in the near field. An important unknown at the present time is the amount of gas present under undisturbed conditions. At one extreme, Salado brine may be fully gas saturated with free gas present at undisturbed pore pressures. At the other extreme, Salado brine may contain only a small quantity of dissolved gas, which comes out of solution only at pressures near atmospheric. The amount of gas in solution will strongly influence how far from the excavations desaturation is occurring due to gas exsolution.

The effect of desaturation on threshold pressure was first studied by Hassler et al. (1943) in the context of oil reservoirs in which production is driven in part by gas exsolution at levels that are insufficient to cause the development of an interconnected gas-filled pore network. This work was later extended to gas-reservoir caprock environments by Thomas et al. (1968) in the context of resealing caprocks once the initial threshold pressure has been exceeded. This research indicates that the impact of desaturation is to reduce threshold pressures progressively until the critical gas saturation is reached, corresponding to the incipient formation of an interconnected, gas-filled pore network (Figure 3). Crossing this critical gas saturation threshold is associated with the initial development of nonzero gas relative permeabilities. At water saturations below the critical gas saturation, threshold pressure is zero. Therefore, the processes of dilatation, drying, and exsolution of dissolved gas from the Salado brine are likely to significantly reduce threshold pressures in the immediate vicinity of the WIPP excavations. These conditions will enhance the ability of waste-generated gas to penetrate and flow through the disturbed rock zone, providing enhanced gas pathways between the room and the higher permeability, nonhalite interbeds. These conditions may also reduce threshold pressure in the halite units of the disturbed rock zone to a level that allows gas penetration into the halite.

6.2 Impact of Fracturing on Threshold Pressure

In low-permeability environments, the presence of fractures frequently dominates hydraulic behavior. In a tight porous material containing small intergranular pores, the existence or introduction of fractures is likely to provide pore space with much larger apertures. The presence of such large-aperture pore space causes a significant reduction in threshold pressure of the total rock mass. Indeed, the presence of natural or induced fractures is considered one of the most important elements in the evaluation of potential caprocks for underground gas storage reservoirs, as the presence of fractures can produce significant leaks (Ibrahim et al., 1970; Katz and Coates, 1973).

Two types of fracturing occur in the vicinity of the WIPP excavations. The first type of fracturing is caused by the redistribution of stress in the immediate vicinity of the excavation. The second type of fracturing is natural, pre-excavation fractures in the relatively brittle anhydrite of Marker Bed 139 and other anhydrite interbeds.

Excavation-related fracturing has been documented by visual observations in holes drilled from the excavations, by geophysical measurements, and by gas injection (Borns and Stormont, 1988; U.S. DOE, 1988). This fracturing includes vertical separations along nonhalite interbeds in the floor and back, arcuate fractures in the floor and back that crosscut a variety of stratigraphic units, and vertical fractures associated with spalling within the ribs. The intensity and extent of fracturing are a function of time and of excavation dimensions. Gas-injection measurements indicate that in the vicinity of a typical drift that has been open for several years, fracturing is most extensive within the first two meters of the excavation (Stormont et al., 1987; Borns and Stormont, 1988). During these tests, gas flow into this zone occurred at test-zone pressures of less than 1 MPa.

In a study of large-diameter drill core, Borns (1985) documented the presence of horizontal and low-angle fractures within Marker Bed 139 that predate the WIPP excavations. While these fractures are much more subtle than those related to the excavation stresses, they are only partially healed and may play an important role in controlling far-field permeability of anhydrite interbeds and the overall hydrologic response of the Salado Formation to the WIPP facility. Borns (1985) concluded that these fractures formed in response to stress cycles related to sedimentation and erosion or in response to deformation in the underlying Castile Formation. In either case, other relatively brittle anhydrite and polyhalite interbeds within the Salado probably responded in a similar fashion. Therefore, it is likely that similar fractures exist in other interbeds as well.

The presence of extensive, excavation-related fracturing adjacent to the WIPP repository will most likely create pore space that is available for the storage of waste-generated gas. In the context of the total room/rock system, this pore space does not actually represent new void volume, but rather represents a redistribution of void volume from the room to the disturbed rock zone. Given the relatively large apertures and corresponding low threshold pressure of fractures, this pore space should be readily accessible to gas that is generated in the adjacent room and will significantly enhance gas flow between the room and the relatively high permeability, nonhalite interbeds. Beyond this zone, the presence of naturally occurring, partially healed fractures in Marker Bed 139 and other similar interbeds may provide potential gas flow pathways that have threshold pressures significantly lower than the 0.5 to 5 MPa range estimated based on empirical correlation with permeability and on the capillary tube model (Section 5).

6.3 Possibility of Zero Permeability in Undeformed, Pure Halite

Because of halite's plastic deformation behavior and low yield strength, it is theoretically not possible to maintain open, interconnected pore space, leading to the general conclusion that halite is impermeable (National Academy of Sciences, 1957). Based on this type of reasoning and on field observations of the occurrence and character of fluids encountered during the mining of salt deposits in Europe, Baar (1977) drew the conclusion that salt deposits are absolutely impermeable at depths of 300 meters or more. Similar conclusions were drawn relative to the Salado Formation during the early stages of the WIPP project (Powers et al., 1978).

Experimental confirmation of absolute zero permeability is not possible. Both laboratory and in situ permeability measurements always have some lower limit of resolution due to equipment limitations. As permeability measurement techniques have been refined and lower limits of resolution achieved, tight rock that was once considered impermeable has been shown to have measurable permeability and measurable heterogeneity at levels below earlier limits of resolution.

Technical arguments concerning the absolute impermeability of halite based on its mechanical behavior rigorously apply only to pure halite. The presence of significant impurities can alter the deformation behavior of halite and absolute impermeability is less likely. Going one step further, continuous interbeds of nonhalite material such as clay or anhydrite may be layers that contain interconnected pore space, which provide thin, low-permeability pathways imbedded within a much larger mass of very low permeability and/or truly impermeable material.

Recent in situ permeability testing in the Salado Formation has encountered a number of relatively pure halite units that maintain large and arbitrary pressures within a test interval for an extended period of time with no observable pressure decay (Beauheim et al., in review; Howarth et al., in press). These units are currently considered to have a permeability of less than approximately 10^{-23} m^2 . At present, it is not possible to determine whether or not these units have a finite permeability (e.g., 10^{-24} m^2) or whether permeability is absolutely zero. Therefore, one must consider the permeability question in the context of a specific problem, which in this case is the penetration and flow of gas under repository conditions. Threshold pressures are likely to be so high in such a tight material that relative permeability to gas of these tight, pure, undeformed halite units is absolutely zero for the range of pressure conditions that are possible in the repository environment.

7. DISCUSSION

Anoxic corrosion and microbial degradation of the WIPP waste may produce sufficient quantities of gas to generate high pressure in the repository. An important objective in assessing the impact of waste-generated gas is evaluating whether or not gas can flow into the surrounding rock, thereby moderating gas pressure. If gas can flow outward, then understanding and quantifying the processes by which this occurs is also very important. If the surrounding rock is fully saturated with brine, then the relative permeability to gas is zero and no gas can flow can occur. In order for gas to flow from a waste repository into the surrounding rock, it must first overcome the sum of the capillary forces resisting penetration (threshold pressure) and the existing brine pressure in the rock pores, and then establish interconnected gas pathways (corresponding to a nonzero relative permeability to gas) that allow outward flow. Threshold pressure is controlled primarily by pore size and pore interconnections. Because pore space in the bedded salt surrounding the WIPP repository is characterized by extremely small apertures, threshold pressures may be quite large. The primary objectives of this study have been to estimate the magnitude of threshold pressure in the bedded salt formation that surrounds the WIPP repository and to evaluate the role that this parameter may play in controlling the outward flow of waste-generated gas.

7.1 Threshold Pressure Estimates for the Salado Formation

Estimates of threshold pressure for the Salado Formation have been made based on an empirical correlation of threshold pressure with intrinsic permeability and on a capillary tube model. The physical rationale behind the correlation approach is that both threshold pressure and intrinsic permeability are controlled, to a large degree, by pore size and pore interconnections. Data for this correlation come primarily from laboratory measurements of threshold pressure and intrinsic permeability on low-permeability caprock materials associated with underground gas-storage studies and on other consolidated rock types. The capillary tube model also comes from underground gas-storage technology and is derived from an idealized capillary tube representation of a porous medium. The permeability correlation and capillary tube model yield generally consistent estimates of threshold pressures for the Salado Formation at the WIPP. These estimates indicate that threshold pressures in relatively pure, undeformed halite may be 20 to 50 MPa, or larger. Threshold pressure of impure halite, mildly deformed halite, and some interbeds is estimated to be on the order of 5 to 25 MPa. Other interbed units, in particular those containing preexisting, partially healed fractures, are estimated to have threshold pressures on the order of 2 to 1/2 MPa, or less. *Because of the compounding effect of low threshold pressure and relatively high intrinsic permeability, these nonhalite interbeds are likely to be the dominant pathways for flow of waste-generated gas away from a pressurized repository.*

The potential importance of nonhalite interbeds can be viewed from a second perspective. If one assumes that the Salado Formation is fully saturated with brine at 12 MPa in the far field and that gas pressure should not exceed lithostatic pressure (15 MPa), then in this far-field region, only lithologic units with a threshold pressure of less than 3 MPa are capable of allowing gas penetration

and the development of interconnected gas-flow paths without exceeding the 15 MPa pressure criteria. Based on estimated threshold pressures for the various Salado lithologies, only the more permeable, nonhalite interbeds are likely to meet this criteria. It should be noted, however, that the lower end of the estimated threshold pressure range for impure halite is 5 MPa, which is close to the 3 MPa criteria for far-field gas penetration and flow. Given the large uncertainties associated with the estimated threshold pressures, it is quite possible that actual threshold pressure in the impure halite of the Salado is less than 3 MPa. This possibility is potentially important because impure halite comprises more than 50 percent of the Salado Formation in the vicinity of the repository and, therefore, represents a significant potential for gas storage.

The discussion thus far has focused primarily on the role of threshold pressure under far-field conditions. Near the repository, a number of processes occur that may significantly reduce threshold pressure. Local fracturing and pore dilatation in response to excavation-related stresses create larger pore apertures (Section 6.2). Desaturation occurs as a result of drying, dilatation, and/or exsolution of gas dissolved in Salado brine under natural conditions (Section 6.1). All of these processes contribute to the development of a zone surrounding the repository that contains pore space that will be readily accessible to waste-generated gas due to significantly decreased threshold pressures. The ready accessibility of the near-field region to gas flow has already been demonstrated at the WIPP by the successful injection of gas in near-field test zones at test zone pressures of less than 1 MPa (Section 6.2). This zone is likely to provide partially desaturated pathways for gas flow from the disposal rooms to nearby nonhalite interbeds that have relatively high permeabilities and low threshold pressures. This near-field zone may also contain significant gas storage potential.

While the threshold pressure estimates discussed in this report are quite useful for formulating concepts and constructing preliminary models of system behavior, the reader is cautioned that there remains considerable uncertainty in these estimates. *These estimates and analyses are based on threshold pressure information from nonsalt rock types and must be confirmed with in situ or laboratory measurements that are specific to the Salado Formation at the WIPP repository.* In particular, such measurements should be directed toward two lithologies, nonhalite interbeds and impure halite. The nonhalite interbeds are the most likely units to have the combination of low threshold pressure and sufficient permeability to allow significant gas flow laterally away from the repository. Because some of the interbed units contain partially healed, pre-existing fractures, laboratory testing may require unusually large samples and in situ testing may be necessary. If threshold pressure in the impure halite is low enough, then these units may provide a relatively large gas-storage volume. Therefore, a second target for WIPP-specific threshold pressure measurements should be impure halite.

7.2 Conceptual Model for Hydrologic Response of the Repository to Waste-Generated Gas

The threshold pressure estimates and related analyses discussed in this report indicate that threshold pressure is likely to be a very important parameter controlling the flow of waste-generated gas from the WIPP repository into the adjacent Salado Formation. Threshold pressure may allow gas penetration and flow along thin, nonhalite interbeds and at the same time prevent significant gas penetration into the halite, which makes up much of the Salado Formation. A conceptual model for the overall system that incorporates this behavior can be summarized as follows. During the early post-closure time period, waste-generated gas (at relatively low pressure) accumulates and is confined to the available pore space within a disposal room and perhaps a thin zone of fractured, depressurized, and partially desaturated rock adjacent to the disposal room. Confinement within this area is provided by a combination of low permeability, moderate to high threshold pressure, and moderate to high pore-fluid pressures in the surrounding rock. However, the surrounding rock is not homogeneous. Heterogeneities in the form of thin, nonhalite interbeds are likely to be a very important factor. In contrast to the high threshold pressure in halite, threshold pressure in the nonhalite interbeds is likely to be low enough for gas to readily penetrate and flow laterally along these units. Also, because of the higher intrinsic permeability of these interbeds, depressurization due to brine drainage is likely to be more extensive than in the halite. Given the combined effects of lower threshold pressure, lower pore fluid pressure, and higher intrinsic permeability, these nonhalite interbeds will be the dominant pathways for flow of waste-generated gas away from the pressurized repository and outward gas flow along the interbeds is likely to be initiated at room pressures well below lithostatic. Gas-flow pathways between the repository and nonhalite interbeds will be provided by the disturbed rock zone and by vertical boreholes (3 to 15 meters in length) drilled for rock bolting and other geotechnical purposes.

The next important step in assessing the impact of waste-generated gas on the WIPP repository is quantifying and testing the conceptual model presented in the previous paragraph. This requires the iterative development of numerical models for assessing system behavior and experimental work to provide data on pertinent physical parameters and processes. Analyses to date indicate strong coupling between the chemical processes controlling gas-generation rates, fluid processes controlling brine flow to disposal rooms and gas flow away from disposal rooms, and mechanical processes controlling room closure and the amount of void space available for gas storage. Assessing the chemical, hydrologic, and mechanical responses the WIPP repository to rising gas pressure is the focus of ongoing modeling and experimental studies at Sandia.

8. REFERENCES

- Asquith, G.B. 1982. *Basic Well Log Analysis for Geologists*. Tulsa, Oklahoma: American Association of Petroleum Geologists.
- Baar, C.A. 1977. *Applied Salt-Rock Mechanics*. Amsterdam: Elsevier Scientific Publishing Company.
- Barker, J.A., and S.S.D. Foster. 1981. "A Diffusion Exchange Model for Solute Movement in Fissured Porous Rock." *Quarterly Journal of Engineering Geology* vol. 14.
- Bear, J. 1972. *Dynamics of Fluids in Porous Media*. New York: American Elsevier Publishing Company, Inc.
- Beauheim, R.L. 1986. *Hydraulic-Test Interpretations for Well DOE-2 at the Waste Isolation Pilot Plant (WIPP) Site*. SAND86-1364. Albuquerque, New Mexico: Sandia National Laboratories.
- Beauheim, R.L., G.J. Saulnier, and J.D. Avis. (in review). *Interpretation of Brine-Permeability Tests of the Salado Formation at the Waste Isolation Pilot Plant*. SAND90-0083. Albuquerque, New Mexico: Sandia National Laboratories.
- Black, S.R., R.S. Newton, and D.K. Shukla. 1983. *Results of Site Validation Experiments, Waste Isolation Pilot Plant (WIPP) Project, Southeastern New Mexico*. TME 3177. Albuquerque, New Mexico: U.S. Department of Energy.
- Borns, D.J. 1985. *Marker Bed 139: A Study of Drillcore from a Systematic Array*. SAND85-0023. Albuquerque, New Mexico: Sandia National Laboratories.
- Borns, D.J., and J.C. Stormont. 1988. *An Interim Report on Excavation Effect Studies at the Waste Isolation Pilot Plant: The Delineation of the Disturbed Rock Zone*. SAND87-1375. Albuquerque, New Mexico: Sandia National Laboratories.
- Borns, D.J., and J.C. Stormont. 1989. "The Delineation of the Disturbed Rock Zone Surrounding Excavations in Salt" in *Proceedings of the 30th U.S. Rock Mechanics Symposia at the University of West Virginia, June 19-22, 1989*. Rotterdam, Netherlands: A.A. Balkeema.
- Brooks, R.H., and A.T. Corey. 1964. *Hydraulic Properties of Porous Media*. Colorado State University, Hydrology Paper No. 3.
- Brush, L.H. 1990. *Test Plan for Laboratory and Modeling Studies of Repository and Radionuclide Chemistry for the Waste Isolation Pilot Plant*. SAND90-0266. Albuquerque, New Mexico: Sandia National Laboratories.
- Calhoun, J.C. 1953. *Fundamentals of Reservoir Engineering*. Norman, Oklahoma: University of Oklahoma Press.

- Carden, P.O., and L. Paterson. 1979. "Physical, Chemical and Energy Aspects of Underground Hydrogen Storage." *International Journal of Hydrogen Energy* vol. 4: 559-569.
- Cosby, B.J., G.M. Hornberger, R.B. Clapp, and T.R. Ginn. 1984. "A Statistical Exploration of the Relationships of Soil Moisture Characteristics to the Physical Properties of Soils." *Water Resources Research* vol. 20, no. 6: 682-690.
- Deal, D.E., and J.B. Case. 1987. *Brine Sampling and Evaluation Program Phase I Report*. DOE/WIPP 87-008. Carlsbad, New Mexico: U.S. Department of Energy, WIPP Project Office.
- de Marsily, G. 1986. *Quantitative Hydrology*. Orlando, Florida: Academic Press.
- Dullien, F.A.L. 1979. *Porous Media, Fluid Transport and Pore Structure*. New York: Academic Press.
- Freeze, R.A., and J.A. Cherry. 1979. *Groundwater*. Englewood Cliffs, New Jersey: Prentice-Hall.
- Golder Associates, Inc. 1987. *Assessment of the Character and Extent of Mechanical Disturbance for Underground Openings in Salt*. BMI/ONWI/C-1. Columbus, Ohio: Office of Nuclear Waste Isolation, Battelle Memorial Institute.
- Hassler, G.L., E. Brunner, and T.J. Deahl. 1943. "The Role of Capillarity in Oil Production." *Petroleum Technology* vol. 155: 155-174.
- Hocott, C.R. 1939. "Interfacial Tension Between Water and Oil Under Reservoir Conditions." *Transactions of the American Association of Mining and Metallurgical Engineers* vol. 132: 184-190.
- Howarth, S.M., E.W. Peterson, P.L. Lagus, K. Lie, S.J. Finley, and J.E. Nowak. (in press). "Interpretation of In-Situ Pressure and Flow Measurements of the Salado Formation at the Waste Isolation Pilot Plant." *Society of Petroleum Engineers*, Paper #21840.
- Hubbert, M.K. 1953. "Entrapment of Petroleum Under Hydrodynamic Conditions." *Association of Petroleum Geologists Bulletin* vol. 37, no. 8: 1954-2026.
- Ibrahim, M.A., M.R. Tek, and D.L. Katz. 1970. *Threshold Pressure in Gas Storage*. Arlington, Virginia: American Gas Association, Inc.
- Jaeger, J.C., and N.G.W. Cook. 1976. *Fundamentals of Rock Mechanics*. London: Chapman and Hall.
- Katz, D.L., and K.H. Coats. 1973. *Underground Storage of Fluids*. Ann Arbor, Michigan: Ulrich's Books, Inc.
- Katz, D.L., and E.R. Lady. 1976. *Compressed Air Storage for Electric Power Generation*. Ann Arbor, Michigan: Ulrich's Books, Inc.

- Katz, D.L., and M.R. Tek. 1970. "Storage of Natural Gas in Saline Aquifers." *Water Resources Research* vol. 6, no. 5: 1515-1521.
- Katz, D.L., D. Cornell, R. Kobayashi, F.H. Poettmann, J.A. Vary, J.R. Elenbaas, and C.F. Weinaug. 1959. *Handbook of Natural Gas Engineering*. New York: McGraw-Hill Book Company.
- Lappin A.R., R.L. Hunter, D.P. Garber, and P.B. Davies. 1989. *Systems Analysis, Long-Term Radionuclide Transport, and Dose Assessments, Waste Isolation Pilot Plant (WIPP), Southeastern New Mexico; March 1989*. SAND89-0462. Albuquerque, New Mexico: Sandia National Laboratories.
- McCabe, W.L., J.C. Smith, and P. Harriott. 1985. *Unit Operations of Chemical Engineering*. New York: McGraw-Hill Book Company.
- McTigue, D.F., S.J. Finley, and E.J. Nowak. 1989. "Brine Transport in Polycrystalline Salt - Field Measurements and Model Considerations." *Transactions, American Geophysical Union* vol. 70, no. 43: 1111.
- Muskat, M. 1949. *Physical Principles of Oil Production*. New York: McGraw-Hill Book Company, Inc.
- National Academy of Sciences. 1957. *The Disposal of Radioactive Waste on Land*. Publication 519. Washington, D.C.: National Academy of Sciences, National Research Council.
- Nowak, E.J., and D.F. McTigue. 1987. *Interim Results of Brine Transport Studies in the Waste Isolation Pilot Plant (WIPP)*. SAND87-0880. Albuquerque, New Mexico: Sandia National Laboratories.
- Nowak, E.J., D.F. McTigue, and R. Beraun. 1988. *Brine Inflow to WIPP Disposal Rooms: Data, Modeling, and Assessment*. SAND88-0112. Albuquerque, New Mexico: Sandia National Laboratories.
- Pandey, G.N., M.R. Tek, and D.L. Katz. 1973. "Studies of Front-End Threshold Pressure Measurements." *American Gas Association Transmission Conference*. T112-T116.
- Peterson, E., P. Lagus, J. Brown, and K. Lie. 1985. *WIPP Horizon In Situ Permeability Measurements Final Report*. SAND85-7166. Albuquerque, New Mexico: Sandia National Laboratories.
- Peterson, E.W., P.L. Lagus, and K. Lie. 1987. *WIPP Horizon Free Field Fluid Transport Characteristics*. SAND87-7164. Albuquerque, New Mexico: Sandia National Laboratories.
- Powers, D.W., S.J. Lambert, S.E. Shaffer, L.R. Hill, and W.D. Weart, eds. 1978. *Geological Characterization Report, Waste Isolation Pilot Plant (WIPP) Site, Southeastern New Mexico*. SAND78-1596. Albuquerque, New Mexico: Sandia National Laboratories.

- Purcell, W.R. 1949. "Capillary Pressures--Their Measurements Using Mercury and the Calculation of Permeability Therefrom." *Transactions of the American Institute of Mining and Metallurgical Engineers* vol. 186: 39-48.
- Rose, W., and W.A. Bruce. 1949. "Evaluation of Capillary Character in Petroleum Reservoir Rock." *Transactions of the American Institute of Mining and Metallurgical Engineers* vol. 186: 127-142.
- Saito, H. 1963. "Capillary Pressure Measurements of Porous Medium by Vapor Pressure Method." in *Sixth World Petroleum Congress, Frankfurt, Germany, June, 1963*. 155-162.
- Saulnier, G.J., and J.D. Avis. 1988. *Interpretation of Hydraulic Tests Conducted in the Waste-Handling Shaft at the Waste Isolation Pilot Plant (WIPP) Site*. SAND88-7001. Albuquerque, New Mexico: Sandia National Laboratories.
- Skokan, C.K., M.C. Pfeifer, G.V. Keller, and H.T. Anderson. 1989. *Studies of Electrical and Electromagnetic Methods for Characterizing Salt Properties at the WIPP Site, New Mexico*. SAND87-7174. Albuquerque, New Mexico: Sandia National Laboratories.
- Stakman, W.P. 1968. "The Relation Between Particle Size, Pore Size and Hydraulic Conductivity of Sand Separates." *International Association of Hydrologic Sciences, Publication No. 82*. 373-383.
- Stein, C.L., and J.L. Krumhansl. 1986. *Chemistry of Brines from the Waste Isolation Pilot Plant (WIPP), Southeastern New Mexico*. SAND85-0897. Albuquerque, New Mexico: Sandia National Laboratories.
- Stormont, J.C., E.W. Peterson, and P.L. Lagus. 1987. *Summary of and Observations About WIPP Facility Horizon Flow Measurements Through 1986*. SAND87-0176. Albuquerque, New Mexico: Sandia National Laboratories.
- Thomas, L.K., D.L. Katz, and M.R. Tek. 1968. "Threshold Pressure Phenomena in Porous Media." *Society of Petroleum Engineers Journal* vol. 8, no. 2: 174-184.
- U.S. Department of Energy. 1988. *Geotechnical Field Data and Analysis Report: June 1986 - June 1987*. DOE/WIPP 87-017. Carlsbad, New Mexico: U.S. Department of Energy, WIPP Project Office.
- Weast, R.C. 1978. *CRC Handbook of Chemistry and Physics*. West Palm Beach, Florida: CRC Press.
- Wyllie, M.R.J., and W.D. Rose. 1950. "Some Theoretical Considerations Related to the Quantitative Evaluation of the Physical Characteristics of Reservoir Rock from Electric Log Data." *Transactions of the American Institute of Mining and Metallurgical Engineers* vol. 189: 105-118.

Wyllie, M.R.J., and M.B. Spangler. 1952. "Application of Electrical Resistivity Measurements to Problem of Fluid Flow in Porous Media." *American Association of Petroleum Geologists Bulletin* vol. 36, no. 2: 359-403.

FEDERAL AGENCIES

U. S. Department of Energy, (5)
Office of Civilian Radioactive
Waste Management
Attn: Deputy Director, RW-2
Associate Director, RW-10
Office of Program Administration
and Resources Management
Associate Director, RW-20
Office of Facilities Siting
and Development
Associate Director, RW-30
Office of Systems Integration
and Regulations
Associate Director, RW-40
Office of External Relations
and Policy
Forrestal Building
Washington, DC 20585

U. S. Department of Energy (3)
Albuquerque Operations Office
Attn: J. E. Bickel
R. Marquez, Director
Public Affairs Division
P.O. Box 5400
Albuquerque, NM 87185

U.S. Department of Energy
Attn: National Atomic Museum Library
Albuquerque Operations Office
P.O. Box 5400
Albuquerque, NM 87185

U.S. Department of Energy (5)
WIPP Project Office (Carlsbad)
Attn: Vernon Daub
J. A. Mewhinney
J. Carr
P.O. Box 3090
Carlsbad, NM 88221

U.S. Department of Energy
Research and Waste Management Division
Attn: Director
P.O. Box E
Oak Ridge, TN 37831

U.S. Department of Energy
Waste Management Division
Attn: R. F. Guercia
P.O. Box 550
Richland, WA 99352

U.S. Department of Energy (1)
Attn: Edward Young
Room E-178
GAO/RCED/GTN
Washington, DC 20545

U.S. Department of Energy (6)
Office of Environmental Restoration
and Waste Management
Attn: Jill Lytle, EM30
Mark Frei, EM-34 (3)
Mark Duff, EM-34
Clyde Frank, EM-50
Washington, DC 20585

U.S. Department of Energy (3)
Office of Environment, Safety
and Health
Attn: Ray Pelletier, EH-231
Kathleen Taimi, EH-232
Carol Borgstrom, EH-25
Washington, DC 20585

U.S. Department of Energy (2)
Idaho Operations Office
Fuel Processing and Waste
Management Division
785 DOE Place
Idaho Falls, ID 83402

U.S. Department of Energy
Savannah River Operations Office
Defense Waste Processing
Facility Project Office
Attn: W. D. Pearson
P.O. Box A
Aiken, SC 29802

U.S. Environmental Protection Agency (2)
Attn: Ray Clark
Office of Radiation Programs (ANR-460)
Washington, DC 20460

U.S. Geological Survey
Branch of Regional Geology
Attn: R. Snyder
MS913, Box 25046
Denver Federal Center
Denver, CO 80225

U.S. Geological Survey
Conservation Division
Attn: W. Melton
P.O. Box 1857
Roswell, NM 88201

U.S. Geological Survey (2)
Water Resources Division
Attn: Russell Livingston
Suite 200
4501 Indian School NE
Albuquerque, NM 87110

U.S. Nuclear Regulatory Commission (4)
Attn: Joseph Bunting, HLEN 4H3 OWFN
Ron Ballard, HLGP 4H3 OWFN
Jacob Philip
NRC Library
Mail Stop 623SS
Washington, DC 20555

BOARDS

Defense Nuclear Facilities Safety Board
Attn: Dermont Winters
Suite 700
625 Indiana Ave., NW
Washington, DC 20004

U.S. Department of Energy
Advisory Committee on Nuclear
Facility Safety
Attn: Meritt E. Langston, AC21
Washington, DC 20585

Nuclear Waste Technical
Review Board (2)
Attn: Dr. Don A. Deere
Dr. Sidney J. S. Parry
Suite 910
1100 Wilson Blvd.
Arlington, VA 22209-2297

Richard Major
Advisory Committee
on Nuclear Waste
Nuclear Regulatory Commission
7920 Norfolk Avenue
Bethesda, MD 20814

STATE AGENCIES

Environmental Evaluation Group (3)
Attn: Library
Suite F-2
7007 Wyoming Blvd., NE
Albuquerque, NM 87109

New Mexico Bureau of Mines
and Mineral Resources (2)
Attn: F. E. Kottolowksi, Director
J. Hawley
Socorro, NM 87801

NM Department of Energy & Minerals
Attn: Librarian
2040 S. Pacheco
Santa Fe, NM 87505

NM Environmental Improvement Division
Attn: Deputy Director
1190 St. Francis Drive
Santa Fe, NM 87503

LABORATORIES/CORPORATIONS

Battelle Pacific Northwest Laboratories (5)
Attn: D. J. Bradley, K6-24
J. Relyea, H4-54
R. E. Westerman, P8-37
H. C. Burkholder, P7-41
L. Pederson, K6-47
Battelle Blvd.
Richland, WA 99352

Savannah River Laboratory (6)
Attn: N. Bibler
E. L. Albenisius
M. J. Plodinec
G. G. Wicks
C. Jantzen
J. A. Stone
Aiken, SC 29801

George Dymmel
SAIC
101 Convention Center Dr.
Las Vegas, NV 89109

INTERA Inc. (5)
Attn: J. F. Pickens
G. A. Freeze
M. Reeves
R. F. Jackson
Suite #300
6850 Austin Center Blvd.
Austin, TX 78731

INTERA Inc.
Attn: Wayne Stensrud
P.O. Box 2123
Carlsbad, NM 88221

IT Corporation (2)
Attn: R. F. McKinney
J. Myers
Regional Office - Suite 700
5301 Central Avenue, NE
Albuquerque, NM 87108

IT Corporation (2)
Attn: D. E. Deal
P.O. Box 2078
Carlsbad, NM 88221

Charles R. Hadlock
Arthur D. Little, Inc.
Acorn Park
Cambridge, MA 02140-2390

Lawrence Berkeley Laboratory
Earth Sciences Division (4)
Attn: J. Long
S. Martel
K. Pruess
C. F. Tsang
1 Cyclotron Road
Berkeley, CA 94720

Los Alamos National Laboratory
Attn: B. Erdal, CNC-11
P.O. Box 1663
Los Alamos, NM 87544

RE/SPEC, Inc. (2)
Attn: W. Coons
P. F. Gnirk
Suite 300
4775 Indian School Rd., NE
Albuquerque, NM 87110-3927

RE/SPEC, Inc. (7)
Attn: L. L. Van Sambeek
G. Callahan
T. Pfeifle
J. L. Ratigan
P.O. Box 725
Rapid City, SD 57709

Center for Nuclear Waste
Regulatory Analysis (4)
Attn: P. K. Nair
Southwest Research Institute
6220 Culebra Road
San Antonio, TX 78228-0510

Science Applications
International Corporation
Attn: Howard R. Pratt,
Senior Vice President
10260 Campus Point Drive
San Diego, CA 92121

Science Applications
International Corporation
Attn: Michael B. Gross
Ass't. Vice President
Suite 1250
160 Spear Street
San Francisco, CA 94105

Systems, Science, and Software (2)
Attn: E. Peterson
Box 1620
La Jolla, CA 92038

Westinghouse Electric Corporation (7)
Attn: Library
Lamar Trego
W. P. Poirer
W. R. Chiquelin
V. F. Likar
D. J. Moak
R. F. Kehrman
P.O. Box 2078
Carlsbad, NM 88221

Weston Corporation (1)
Attn: David Lechel
Suite 1000
5301 Central Avenue, NE
Albuquerque, NM 87108

UNIVERSITIES

University of Arizona
Attn: J. G. McCray
Department of Nuclear Engineering
Tucson, AZ 85721

University of British Columbia (2)
Attn: R. A. Freeze
J. L. Smith
Department of Geological Sciences
6339 Stores Road
Vancouver, British Columbia V6T 2B4
CANADA

University of New Mexico (2)
Geology Department
Attn: Library
Albuquerque, NM 87131

Pennsylvania State University
Materials Research Laboratory
Attn: Della Roy
University Park, PA 16802

Texas A&M University
Center of Tectonophysics
College Station, TX 77840

G. Ross Heath
College of Ocean
and Fishery Sciences
University of Washington
Seattle, WA 98195

University of Virginia
Attn: G. M. Hornberger
Department of Environmental Sciences
Clark Hall
Charlottesville, VA 22903

INDIVIDUALS

Dennis W. Powers
Star Route Box 87
Anthony, TX 79821

LIBRARIES

Thomas Brannigan Library
Attn: Don Dresp, Head Librarian
106 W. Hadley St.
Las Cruces, NM 88001

Hobbs Public Library
Attn: Ms. Marcia Lewis, Librarian
509 N. Ship Street
Hobbs, NM 88248

New Mexico State Library
Attn: Ms. Ingrid Vollenhofer
P.O. Box 1629
Santa Fe, NM 87503

New Mexico Tech
Martin Speere Memorial Library
Campus Street
Socorro, NM 87810

Pannell Library
Attn: Ms. Ruth Hill
New Mexico Junior College
Lovington Highway
Hobbs, NM 88240

WIPP Public Reading Room
Attn: Director
Carlsbad Public Library
101 S. Halagueno St.
Carlsbad, NM 88220

Government Publications Department
General Library
University of New Mexico
Albuquerque, NM 87131

THE SECRETARY'S BLUE RIBBON PANEL
ON WIPP

Dr. Thomas Bahr
New Mexico Water Resources Institute
New Mexico State University
Box 3167
Las Cruces, NM 88003-3167

Mr. Leonard Slosky
Slosky and Associates
Suite 1400
Bank Western Tower
1675 Tower
Denver, CO 80202

Mr. Newal Squyres
Holland & Hart
P.O. Box 2527
Boise, ID 83701

Dr. Arthur Kubo
Vice President
BDM International, Inc.
7915 Jones Branch Drive
McLean, VA 22102

Mr. Robert Bishop
Nuclear Management Resources Council
Suite 300
1776 I Street, NW
Washington, DC 20006-2496

NATIONAL ACADEMY OF SCIENCES,
WIPP PANEL

Dr. Charles Fairhurst, Chairman
Department of Civil and
Mineral Engineering
University of Minnesota
500 Pillsbury Dr., SE
Minneapolis, MN 55455

Dr. John O. Blomeke
Route 3
Sandy Shore Drive
Lenoir City, TN 37771

Dr. John D. Bredehoeft
Western Region Hydrologist
Water Resources Division
U.S. Geological Survey (M/S 439)
345 Middlefield Road
Menlo Park, CA 94025

Dr. Karl P. Cohen
928 N. California Avenue
Palo Alto, CA 94303

Dr. Fred M. Ernsberger
250 Old Mill Road
Pittsburgh, PA 15238

Dr. Rodney C. Ewing
Department of Geology
University of New Mexico
200 Yale NE
Albuquerque, NM 87131

B. John Garrick
Pickard, Lowe & Garrick, Inc.
2260 University Drive
Newport Beach, CA 92660

John W. Healy
51 Grand Canyon Drive
Los Alamos, NM 87544

Leonard F. Konikow
U.S. Geological Survey
431 National Center
Reston, VA 22092

Jeremiah O'Driscoll
505 Valley Hill Drive
Atlanta, GA 30350

Dr. D'Arcy A. Shock
233 Virginia
Ponca City, OK 74601

Dr. Christopher G. Whipple
Clement International
Suite 1380
160 Spear Street
San Francisco, CA 94105

Dr. Peter B. Myers, Staff
Director
National Academy of Sciences
Committee on Radioactive
Waste Management
2101 Constitution Avenue
Washington, DC 20418

Dr. Geraldine Grube
Board on Radioactive Waste
Management
GF456
2101 Constitution Avenue
Washington, DC 20418

Dr. Ina Alterman
Board on Radioactive Waste
Management
GF462
2101 Constitution Avenue
Washington, DC 20418

FOREIGN ADDRESSES

Studiecentrum Voor Kernenergie
Centre D'Energie Nucleaire
Attn: Mr. A. Bonne
SCK/CEN
Boeretang 200
B-2400 Mol
BELGIUM

Mr. D. J. Pascoe
Environment Canada
Ontario Region/G&P
25 St. Clair Avenue East
Toronto, Ontario M4T 1M2
CANADA

Atomic Energy of Canada, Ltd. (2)
Whiteshell Research Estab.
Attn: Peter Haywood
John Tait
Pinewa, Manitoba, CANADA
ROE 1LO

Dr. D. K. Mukerjee
Ontario Hydro Research Lab
800 Kipling Avenue
Toronto, Ontario, CANADA
M8Z 5S4

Mr. Francois Chenevier, Director (2)
ANDRA
Route du Panorama Robert Schumann
B.P.38
92266 Fontenay-aux-Roses Cedex
FRANCE

OECD Nuclear Energy Agency (3)
Attn: Dr. Hong L. Chang
Dr. Daniel A. Galson
Mr. Jean-Pierre Olivier
Division of Radiation Protection
and Waste Management
38, Boulevard Suchet
75016 Paris, FRANCE

Claude Sombret
Centre D'Etudes Nucleaires
De La Vallee Rhone
CEN/VALRHO
S.D.H.A. BP 171
30205 Bagnols-Sur-Ceze
FRANCE

Gesellschaft fur Reaktorsicherheit
Attn: Peter Bogorinski
Schwertnergasse 1
500 Koln 1
FEDERAL REPUBLIC OF GERMANY

Bundesministerium fur Forschung und
Technologie
Postfach 200 706
5300 Bonn 2
FEDERAL REPUBLIC OF GERMANY

Bundesanstalt fur Geowissenschaften
und Rohstoffe
Attn: Michael Langer
Postfach 510 153
3000 Hannover 51
FEDERAL REPUBLIC OF GERMANY

Hahn-Meitner-Institut fur Kernforschung
Attn: Werner Lutze
Glienicke Strasse 100
100 Berlin 39
FEDERAL REPUBLIC OF GERMANY

Institut für Tieflagerung (4)
Attn: K. Kuhn
Theodor-Heuss-Strasse 4
D-3300 Braunschweig
FEDERAL REPUBLIC OF GERMANY

Kernforschung Karlsruhe
Attn: K. D. Closs
Postfach 3640
7500 Karlsruhe
FEDERAL REPUBLIC OF GERMANY

Physikalisch-Technische Bundesanstalt
Attn: Peter Brenneke
Postfach 33 45
D-3300 Braunschweig
FEDERAL REPUBLIC OF GERMANY

D. R. Knowles
British Nuclear Fuels, plc
Risley, Warrington, Cheshire WA3 6AS
1002607 GREAT BRITAIN

Shingo Tashiro
Japan Atomic Energy Research Institute
Tokai-Mura, Ibaraki-Ken
319-11 JAPAN

Netherlands Energy Research Foundation
ECN (2)
Attn: Tuen Deboer, Mgr.
L. H. Vons
3 Westerduinweg
P.O. Box 1
1755 ZG Petten, THE NETHERLANDS

Svensk Kärnbränsleforsörjning AB
Attn: Fred Karlsson
Project KBS
Kärnbränslesakerhet
Box 5864
10248 Stockholm, SWEDEN

KEMAKTA Consultants Co.
Attn: Mark Elert
Pipersgatan 27
S-112 28
Stockholm
SWEDEN

SANDIA INTERNAL

400 L. D. Tyler
1511 D. F. McTigue
1514 C. M. Stone
3141 S. A. Landenberger (5)
3151 Supervisor (3)
3154-1 C. L. Ward, (10) for DOE/OSTI
6000 V. L. Dugan, Acting
6232 W. R. Wawersik
6233 R. T. Cygan
6300 T. O. Hunter, Acting
6310 T. E. Blejwas, Acting
6313 L. E. Shephard
6313 R. J. Glass
6340 W. D. Weart
6340 S. Y. Pickering
6340A A. R. Lappin
6341 R. C. Lincoln
6341 Staff (9)
6341 Sandia WIPP Central Files (10)
6342 D. R. Anderson
6342 Staff (11)
6343 T. M. Schultheis
6343 Staff (2)
6344 E. D. Gorham
6344 P. B. Davies (30)
6344 Staff (10)
6345 B. M. Butcher, Acting
6345 Staff (9)
6346 J. R. Tillerson
6346 Staff (7)
7223 C. A. Gotway
8524 J. A. Wackerly (SNLL Library)
9300 J. E. Powell
9310 J. D. Plimpton
9320 M. J. Navratil
9325 L. J. Keck (2)
9330 J. D. Kennedy
9333 O. Burchett
9333 J. W. Mercer
9334 P. D. Seward

Dist-8